Optimal scheduling of CCHP-based resilient energy distribution system considering active microgrids' multi-carrier energy transactions

Optimal scheduling of CCHP-based resilient energy distribution system considering active microgrids' multi-carrier energy transactions

Majid Armioun [a], Mehrdad Setayesh Nazar [a], Miadreza Shafie-khah [b], Pierluigi Siano [c,d]

[a] *Faculty of Electrical Engineering, Shahid Beheshti University, Tehran, Iran*

[b] *School of Technology and Innovations, University of Vaasa, 65200 Vaasa, Finland*

[c] *Department of Management & Innovation Systems, University of Salerno, Fisciano, SA 84084, Italy*

[d] *Department of Electrical and Electronic Engineering Science, University of Johannesburg, Johannesburg 2006, South Africa*

Abstract

This paper introduces a two-stage two-level optimization method for optimal day-ahead and real-time scheduling of multicarrier energy distribution systems and microgrids. The model considers the incentive-based and pricebased demand response programs to encourage microgrids to transact electrical, heating, and cooling energy carriers with the energy distribution system, which is named hereafter as the energy system. Further, the model formulates the resilient operation of the energy system considering the energy transactions with the electrical, heating, and cooling markets. The main contribution of this paper is the integration of demand response procedures of microgrids in energy transactions with the energy system considering the switching of electrical switches and heating and cooling control valves. The optimization process is another contribution of this paper that is decomposed into two stages that consist of day-ahead and real-time horizons. The first stage is also decomposed into two levels that determine the optimal scheduling of the energy system and microgrids in day-ahead markets. The second stage is comprised of two levels that commit the energy system and microgrids resources. A resiliency index is proposed to assess the resiliency of the energy system in shock conditions. The proposed method was simulated for the 123-bus test system. Different types of microgrids, incentive-based and price-based demand response processes were considered. Simulation results confirmed that the proposed method can reduce the costs of residential, industrial, and commercial microgrids by about 4.47%, 3.88%, and 5.47% concerning only the real-time pricing process. Further, the model can increase the aggregated benefits of the energy system in the day-ahead and real-time markets by about 0.608 Million Monetary Units (MMUs) and 1.10 MMUs, respectively.

1. Introduction

1.1. Literature review

The optimal operation of multi-carrier energy distribution systems is an important issue considering the energy transactions of these systems with the multi-carrier energy markets and microgrids. The energy system can be equipped with multi-carrier Distributed Energy Resources (DERs) and can utilize different demand response programs to encourage the Microgrids (MGs) to change their load and energy transaction profiles. The multi-carrier energy transactions of microgrids

Nomenclature

Abbreviation

ARIMA	Autoregressive Integrated Moving Average
CCHP	Combined Cool, Heat and Power.
CCP	Chance-Constrained Programming
CVaR	Conditional Value-at-Risk
DA	Day-Ahead
DER	Distributed Energy Resources
DRP	Demand Response Program
DSO	Distribution System Operator
ESS	Electrical Energy Storage
GA	Genetic Algorithm
IBDR	Incentive-Based Demand Response
IBEDRP	Incentive-Based Electrical Demand Response Program
IBHDRP	Incentive-Based Heating Demand Response Program
IBCDRP	Incentive-Based Cooling Demand Response Program
MG	Micro Grid
MILP	Mixed Integer Linear Programming
MINLP	Mixed Integer Non-Linear Programming
MIQP	Mixed Integer Quadratic Programming
MPEC	Mathematical Programming with Equilibrium Constraints
MCESRI	Multi-Carrier Energy System Resiliency Index
PBEDRP	Price-Based Electrical Demand Response Program
PBHDRP	Price-Based Heating Demand Response Program
PBCDRP	Price-Based Cooling Demand Response Program
PHEV	Plug-in Hybrid Electrical Vehicle
PSO	Particle Swarm Optimization

Sets

J	Set of MGs that participated in IBEDRP
J'	Set of MGs that participated in IBHDRP
J"	Set of MGs that participated in IBCDRP
G	Set of MGs that participated in PBEDRP
G'	Set of MGs that participated in PBHDRP
G"	Set of MGs that participated in PBCDRP

Parameters

A^{PV}	Area of photovoltaic array
η	Photovoltaic array conversion efficiency
I	Solar irradiation
t_0	Outside air temperature
$\gamma_{DS}(t)$	Electrical generation costs of energy system
$SU_{i\,DS}(t)$	Startup costs of the energy system
$\gamma'_{DS}(t)$	Heating energy generation costs of energy system
$\gamma''_{DS}(t)$	Cooling energy generation costs of the energy system
$EENSC_{DS}(t)$	DSO's electrical energy not supplied costs
$HENSC_{DS}(t)$	DSO's heating energy not supplied costs
$CENSC_{DS}(t)$	DSO's cooling energy not supplied costs
$ENP^{DG}_{CO2}(t)$, $ENP^{DG}_{SO2}(t)$, $ENP^{DG}_{NOx}(t)$	Volume of CO2, SO2, and NOx pollution of the distributed generation unit
$ENP^{Market}_{CO2\ Market}(t)$, $ENP^{Market}_{SO2\ Market}(t)$, $ENP^{Market}_{NOx\ Market}(t)$	Volume of CO2, SO2, and NOx pollution of electrical wholesale market generation unit
$P^{L}_{DS}(t)$	Active power of DSO's loads
$H^{L}_{DS}(t)$	Heating power of DSO's loads
$R^{L}_{DS}(t)$	Cooling power of DSO's loads
$\gamma_{MG}(t)$	Cost of energy generation of MG
$\gamma''_{MG}(t)$	Cost of cooling energy generation of MG
$\gamma'_{MG}(t)$	Cost of heating energy generation of MG
$\gamma_{MG}(t)$	Cost of electrical energy generation of MG
$EENSC_{S\,MG}(t)$	Electrical energy not supplied costs of MG
$HENSC_{S\,MG}(t)$	Heating energy not supplied costs of MG
$CENSC_{S\,MG}(t)$	Cooling energy not supplied costs of MG
$ENP^{DG}_{CO2}(t)$, $ENP^{DG}_{SO2}(t)$, $ENP^{DG}_{NOx}(t)$	Volume of CO2, SO2, and NOx pollution of MG's distributed generation unit
$H^{L}_{MG}(t)$	MG's heating power of loads
$H^{ACH}_{MG}(t)$	MG's heating energy consumption of absorption chiller
$R^{L}_{m,s\ MG}$	MG's cooling power of loads
$ECIC_{DS}(t)$	Electrical energy not supplied costs of energy system
$HCIC_{DS}(t)$	Heating energy not supplied costs of energy system
$CCIC_{DS}(t)$	Cooling energy not supplied costs of energy system
$P_{Critical}, H_{Critical}, R_{Critical}$	Critical electrical loads, critical heating loads, and critical cooling loads
$ECIC_{MG}(t)$	MG's electrical consumer interruption costs
$HCIC_{MG}(t)$	MG's heating consumer interruption costs
$CCIC_{MG}(t)$	MG's heating consumer interruption costs
vci	Cut-in wind velocity
vr	Nominal wind velocity
vco	Cut-out wind velocity
vwind	wind velocity
T	Number of operational scheduling hours of the energy system
DSDAS	Number of energy system day-ahead operating scenarios
DSRTS	Number of energy system real-time operating scenarios
NDG	Number of energy system DGs
NHDER	Number of energy system heating DERs
NCDER	Number of energy system's cooling DERs
NIDG	Number of energy system intermittent DGs
NEL	Number of electrical load buses of the energy system
NHL	Number of heating load buses of the energy system
NCL	Number of cooling load buses of the energy system
NRMG	Number of residential MGs
NCMG	Number of commercial MGs
NIMG	Number of industrial MGs
NEIBDR	Number of electrical loads participating in IBEDRP
NHIBDR	Number of heating loads participating in IBHDRP
NCIBDR	Number of cooling loads participating in IBCDRP
MGDAS	Number of MG's day-ahead operating scenarios
MGRTS	Number of MG's real-time operating scenarios
NDG'	Number of MGS' DGs
NHRMG	Number of heating energy resources of MGs
NCRMG	Number of cooling energy resources of MGs
NIDG'	Number of MGs' intermittent DGs
NEL'	Number of electrical load buses of MGs
NHL'	Number of electrical load buses of MGs
NCL'	Number of electrical load buses of MGs
NRTSS	Number of energy system real-time simulation steps
NNCSW	Number of energy system electric switches
NNCHV	Number of energy system heating energy control valve
NNCCV	Number of energy system cooling energy control valve
NCEL	Number of critical electrical load buses of the energy system
NCHL	Number of critical heating load buses of the energy system
NCCL	Number of critical cooling load buses of the energy system

Variables

$AELRC(r,t)$	Actual electrical load reduction of residential MG
$SELRC(r,t)$	Submitted value of electrical load reduction of residential MG
$AELCC(r,t)$	Actual electrical load reduction of commercial MG
$SELCC(r,t)$	Submitted value of electrical load reduction of commercial MG
$AELIC(r,t)$	Actual electrical load reduction of industrial MG
$SELIC(r,t)$	Submitted value of electrical load reduction of industrial MG

$AHLRC(r,t)$ Actual heating load reduction of residential MG

$SHLRC(r,t)$ Submitted value of heating load reduction of residential MG

$AHLCC(r,t)$ Actual heating load reduction of commercial MG

$SHLCC(r,t)$ Submitted value of heating load reduction of commercial MG

$AHLIC(r,t)$ Actual heating load reduction of industrial MG

$SHLIC(r,t)$ Submitted value of heating load reduction of industrial MG

$ACLRC(r,t)$ Actual cooling load reduction of residential MG

$SCLRC(r,t)$ Submitted value of cooling load reduction of residential MG

$ACLCC(r,t)$ Actual cooling load reduction of commercial MG

$SCLCC(r,t)$ Submitted value of cooling load reduction of commercial MG

$ACLIC(r,t)$ Actual cooling load reduction of industrial MG

$SCLIC(r,t)$ Submitted value of cooling load reduction of industrial MG

$\mathbb{Z}_{DS}^{DA}(t)$ Objective function of the energy distribution system

$P_{i\,DS}^{EDER}(t)$ Electrical power generation of DSO's distributed generation units

$K_{i\,DS}(t)$ Binary decision variable commitment of DSO's electrical DERs

$H_{DS}^{HDER}(t)$ Heating power generation of DSO's DERs

$K'_{DS}(t)$ Binary decision variable commitment of DSO's heating DERs

$R_{DS}^{CDER}(t)$ Cooling power generation of DSO's DERs

$K''_{DS}(t)$ Binary decision variable commitment of DSO's cooling DERs

$C_{MG}^{IBEDR\_DA}(t)$ DSO's costs of IBEDRP paid to MGs

$C_{MG}^{IBHDR\_DA}(t)$ DSO's costs of IBHDRP paid to MGs

$C_{MG}^{IBCDR\_DA}(t)$ DSO's costs of IBCDRP paid to MGs

$C_{MG}^{PBEDR\_DA}(t)$ DSO's costs of PBEDRP paid to MGs

$C_{MG}^{IBHDR\_DA}(t)$ DSO's costs of PBHDRP paid to MGs

$C_{MG}^{IBCDR\_DA}(t)$ DSO's costs of PBCDRP paid to MGs

$C_{DS}^{IMPORT\_DA}(t)$ DSO's costs of electrical energy purchased from the electricity market

$C_{DS}^{PHEVPL\_DA}(t)$ DSO's costs of electrical energy purchased from PHEV parking lots

$B_{DS}^{PHEVPL\_DA}(t)$ Benefits of electrical energy sold to PHEV parking lots

$C_{DS}^{E\_IMPORT\_DA}(t)$ DSO's costs of imported electricity to the electricity wholesale market

$B_{DS}^{E\_EXPORT\_DA}(t)$ DSO's benefits of exported electricity from the electricity wholesale market

$C_{DS}^{H\_IMPORT\_DA}(t)$ DSO's costs of imported heating energy to the heating energy market

$B_{DS}^{H\_EXPORT\_DA}(t)$ DSO's benefits of exported electricity from the heating energy market

$C_{DS}^{C\_IMPORT\_DA}(t)$ DSO's costs of imported electricity to the cooling energy market

$B_{DS}^{C\_EXPORT\_DA}(t)$ DSO's benefits of exported electricity from the cooling energy market

$C_{DS}^{IDG}(t)$ Operating costs of DSO's intermittent electricity facilities

$VC_{MG}^{PBEDR\_DA}(t)$ Variable costs of PBEDRP paid to MGs

$VC_{MG}^{PBHDR\_DA}(t)$ Variable costs of PBHDRP paid to MGs

$VC_{MG}^{PBCDR\_DA}(t)$ Variable costs of PBCDRP paid to MGs

$P_{DS}^{E\_Market}(t)$ Exported/imported power to/from the electricity market

$P_{DS}^{CCHP}(t)$ Generated electrical power of CCHP

$P_{DS}^{ESS}(t)$ Transacted electrical power with electrical energy storages

$P_{DS}^{CCH}(t)$ Electricity consumption of the compressed chiller

$H_{DS}^{CCHP}(t)$ Generated heating power of DSO's CCHP units

$H_{DS}^{H\_Market}(t)$ Exported/imported heating power to/from the heating energy market

$H_{DS}^{Boiler}(t)$ Generated heating power of the boiler

$H_{DS}^{TES}(t)$ Heating power transactions of thermal energy storages

$H_{DS}^{ACH}(t)$ Heating energy consumption of absorption chiller

$H_{DS}^{PBDR}(t)$ PBHDRP heating loads

$R_{DS}^{CCHP}(t)$ Generated cooling power of DSO's CCHP units

$R_{DS}^{C\_Market}(t)$ Exported/imported power to/from the cooling market

$R_{DS}^{ACH}(t)$ Generated cooling power of absorption chillers

$R_{DS}^{CCH}(t)$ Generated cooling power of compressed chillers

$R_{DS}^{PBDR}(t)$ PBCDRP cooling loads

$P_{MG}(t)$ Generated electrical power of MG's DERs

$K_{MG}(t)$ Binary decision variable of unit commitment of MG's electrical DERs

$H_{MG}^{HDER}(t)$ Generated heating power of MG's DERs

$K'_{MG}(t)$ Binary decision variable of unit commitment of MG's heating DERs

$RH_{MG}^{CDER}(t)$ Generated heating power of MG's DERs

$K''_{MG}(t)$ Binary decision variable of unit commitment of MG's cooling DERs

$B_{MG}^{IBEDR\_DA}(t)$ MGs benefits of IBEDRP

$B_{MG}^{IBHDR\_DA}(t)$ MGs benefits of IBHDRP

$B_{MG}^{IBCDR\_DA}(t)$ MGs benefits of IBCDRP

$B_{MG}^{PBEDR\_DA}(t)$ MGs benefits of PBEDRP

$B_{MG}^{PBHDR\_DA}(t)$ MGs benefits of PBHDRP

$B_{MG}^{PBCDR\_DA}(t)$ MGs benefits of PBCDRP

$C_{MG}^{IMPORT\_DA}(t)$ MG's costs of electrical energy purchased from the distribution system

$B_{MG}^{EXPORT\_DA}(t)$ MG's benefit of electrical, heating, and cooling energy sold to the distribution system

$C_{MG}^{IDG}(t)$ operating costs of MG's intermittent electricity facilities

$Penalty_{MG}^{IBEDR\_DA}(t)$ Penalty costs of MG's IBEDRP

$Penalty_{MG}^{IBHDR\_DA}(t)$ Penalty costs of MG's IBHDRP

$Penalty_{MG}^{IBCDR\_DA}(t)$ Penalty costs of MG's IBCDRP

$P_{MG}^{DG}(t)$ Generated electrical power of distributed generation units of MG

$P_{MG}^{DSO}(t)$ MG's exported (imported) power to (from) the electrical distribution system

$P_{MG}^{CCHP}(t)$ Generated electrical power of MG's CCHP

$P_{MG}^{PHEV}(t)$ Transacted electrical power with MG's PHEV parking lots

$P_{MG}^{PBDR}(t)$ Price-based demand response programs MG's electrical load

$P_{MG}^{CCH}(t)$ Electricity consumption of MG's compressed chiller

$H_{MG}^{CCHP}(t)$ generated heating power of MG's CCHP units

$H_{MG}^{Boiler}(t)$ generated heating power of MG's boiler

$H_{MG}^{PBDR}(t)$ MG's PBHDRPs heating loads

$R_{s\,MG}^{CCHP}(t)$ Generated cooling power of MG's CCHP units

$R_{s\,MG}^{ACH}(t)$ Generated cooling power of absorption chillers

$R_{s\,MG}^{CCH}(t)$ Generated cooling power of compressed chillers

$R_{b,s\,MG}^{PBDR}(t)$ MG's PBCDRPs cooling loads

P_0, H_0, R_0 Unserved loads of electrical, heating, and cooling systems

X^{EL}, X^{HCV}, X^{CCV} Switching status of electrical switches, heating and cooling system control valves

with the energy system can change the volume and availability of DERs' of the energy system in normal and shock conditions. Further, the switching of electrical switches and heating and cooling valves can change the energy flow of the energy system's resources, which should be considered a resilient operational scheduling tool.

The optimal operational scheduling of energy systems is highly considered in recent papers and the literature as described in the following.

Ref. [1] proposed a bi-level active and reactive power scheduling process. The model considered the locational marginal prices. The upper-level problem determined the optimal dispatch of Combined Cooling, Heating, and Power (CCHP) units; meanwhile, the lower-level problem performed the market-clearing process. The model utilized the Big-M and duality theories to convert the bi-level Mathematical Programing with Equilibrium Constraints (MPEC) model to a single-level mixed-integer second-order cone-programming model. The case studies presented that the energy efficiency and renewable energy contributions were increased. Ref. [2] introduced a joint chance constraint method to minimize the operating costs of power-to-gas facilities and capture carbon dioxide. The uncertainties of intermittent electricity generation units, electricity market price, and loads were modeled. The proposed model reduced carbon emissions by about 50%. However, the power-to-gas process increased the operating costs of the system by about 10%. Refs. [1,2] did not consider the resiliency of the energy system and the switching process of control valves.

Ref. [3] explored an optimization process for power, cooling, heating, and hydrogen energy systems. The model assessed a Mixed-Integer Nonlinear Programming (MINLP) model to minimize the capital costs, operating costs, maintenance costs, and environmental emissions. The Pareto optimal solution was found using the proposed model, in which the degree of objective function satisfaction was about 0.75. Further, the method revealed that the utilization of energy storage reduced environmental emissions by about 45%. Ref. [4] assessed an adiabatic compressed air energy storage technology for CCHP dispatch. The model considered the temperature dynamic behavior of the energy storage facilities and Mixed-Integer Linear Programming (MILP) was used to solve the problem. The proposed model reduced the operating costs of the system by about 13.7% if compared with the conventional method optimization process. Further, the system costs were reduced by about 48.35%, when the compressed air energy storage was utilized. Refs. [3,4] did not model microgrid energy transactions with the energy system and heating and cooling markets.

Ref. [5] proposed a multi-objective problem model to minimize operating costs and emission pollution of a CCHP-based microgrid. The model utilized a scenario-based approach and robust optimization to consider the uncertainties. The output results indicated that the model reduced the emission cost by about 55%. However, the optimization process increased the operating costs by about 11% to achieve zero-level risk. Ref. [6] showed that the incentive-based participation of multi-energy microgrids in energy markets reduced the operating costs by about 4.3$. The model considered energy storage and intermittent power generation facilities and Chance-Constrained Programming (CCP) was used to solve the problem. The optimization method increased the operating costs by about 4.3% to guarantee the reliable performance of the system with a probability of 98%. Refs. [5,6] did not model the resilient operation of the system and the switching process of control valves.

Ref. [7] explored different Incentive-Based Demand Response (IBDR) alternatives for microgrids. The resilient response of the system was simulated and different economy and reliability indices were studied for normal and resilient conditions. The model considered the commitment of microgrids, which minimized the microgrids' energy procurement costs; meanwhile, maximized their profits. The proposed model increased the expected profit of the system by about 4% and 2.7% for normal and resilient conditions, respectively. Ref. [8] utilized an incentive-based trading mechanism for a CCHP-based MG cluster utilizing a decentralized solution model. An asymmetric Nash bargaining theory was used to determine the benefit of microgrids. The model utilized a contribution rate that was defined as the economic value of exchanged energy. Then, based on the contribution rates of microgrids, their benefits were determined. Refs. [7,8] did not assess the heating and cooling energy transactions of MGs with the energy system.

Ref. [9] introduced a coordinated operation of a CCHP-based industrial energy park to minimize operation costs and CO_2 emissions. A hybrid stochastic/information gap decision theory was used to solve the problem. The uncertainties of intermittent energy generations, loads, and prices were considered. The results revealed that total operation cost and emission pollution were reduced by about 3.1%, and 2.2%, respectively. Ref. [10] explored an integrated model for scheduling intermittent power generation facilities, demand response alternatives, energy storage, and electric vehicles. The model considered gas, electrical, and heat markets and a robust optimization method was used to solve the problem. The process reduced operational costs by about 14.2% considering the electric vehicle contributions. Further, the model reduced the operating costs by about 13% using demand response procedures. Refs. [9,10] did not consider the resiliency operation of the energy system. Ref. [11] proposed an optimization procedure for a CCHP-based system that utilized compressed air energy storage and an internal combustion engine. The model used a bi-level optimization process, in which the upper level optimized the active equipment capacity of the system and the lower level minimized the primary energy saving ratio and energy consumption cost. The model reduced the primary energy saving ratio by 12.07%. Ref. [12] evaluated a real-time demand response process with optimal scheduling of CCHP-based microgrids. The objective functions minimized operating costs and carbon emissions. The model considered real-time demand response processes, energy hubs, and intermittent energy generation facilities. The method found the optimal Pareto solutions using the max-min fuzzy and weighted sum approach. The output revealed that the carbon emission and operation costs were reduced by 2.26% and 3.97%, respectively. Refs. [11,12] did not model heating and cooling energy markets and the resiliency of energy systems.

Ref. [13] proposed an optimization process that preserved information privacy and considered the independent scheduling of microgrids. The uncertainties of multi-carrier energy loads and intermittent energy generations were modeled and a CCP method was used to solve the problem. Further, the cost allocation was modeled to increase the stability of the microgrids coalition. Ref. [14] presented a meta-heuristic optimization method for optimal design and energy management of DERs in microgrids. The model considered energy storage, boiler, and intermittent power generation facilities. A Particle Swarm Optimization (PSO) process was carried out. The process reduced fuel consumption and emission pollution by about 6.2% and 46.8%, respectively. Refs. [13,14] did not model the heating and cooling markets, resilience operating conditions of the energy system, and switching of control valves.

Ref. [15] introduced a two-stage CCHP microgrid energy management process that comprised by economic dispatch and real-time adjustment processes. The first-stage and second-stage problems were solved using MILP and Mixed Integer Quadratic Programming (MIQP) solvers, respectively. The proposed model reduced the system's costs by about 16.51% and 11.05% concerning the following thermal load mode and the following electric load mode, respectively. Ref. [16] proposed an optimization process for active power, reactive power, and topology of the system to minimize operating costs, energy loss, and emission pollutants. The optimization process utilized a hybrid big crunch machine to optimize the problem. The proposed method reduced the operating costs of the system by about 49.03% concerning the custom optimal power flow method. Refs. [15,16] did not explore the optimal resilient operational scheduling of energy systems considering the heating and cooling markets.

Ref. [17] assessed a dynamic robust optimal scheduling process that

Table 1
Comparison of the proposed method with other papers.

References		1	2	3	4	5	6	7	8	9	10	11	12	13	14	15	16	17	18	19	20	21	22	Proposed Approach
Heating market and/or cooling market		✘	✔	✘	✘	✘	✘	✘	✘	✔	✘	✘	✘	✘	✘	✘	✘	✘	✘	✘	✘	✘	✘	✔
Switching of control valves		✘	✘	✘	✘	✘	✘	✘	✘	✘	✘	✘	✘	✘	✘	✘	✘	✘	✘	✘	✘	✘	✘	✔
Switching of electrical switches		✘	✘	✘	✘	✘	✘	✘	✘	✘	✘	✘	✘	✘	✘	✘	✘	✘	✘	✘	✘	✘	✘	✔
Resilient operation of system		✘	✘	✘	✘	✘	✘	✘	✘	✘	✘	✘	✘	✘	✘	✘	✘	✘	✘	✘	✘	✘	✘	✔
Method	**MILP**	✔	✘	✘	✔	✔	✘	✔	✘	✘	✘	✘	✘	✘	✘	✘	✘	✔	✘	✘	✘	✘	✘	✘
	MINLP	✘	✘	✔	✘	✘	✘	✘	✘	✘	✘	✘	✘	✘	✘	✘	✔	✘	✘	✘	✘	✘	✘	✘
	Heuristic	✘	✔		✘	✘	✔	✘	✔	✔	✔	✔	✔	✔	✔	✔	✘	✘	✔	✔	✔	✔	✔	✔
Model	**Determ.**	✔	✘	✔	✔	✘	✘	✔	✔	✘	✘	✔	✔	✔	✔	✔	✘	✘	✔	✘	✘	✔	✔	✘
	Stoch.	✘	✔	✘	✘	✔	✔	✘	✘	✔	✔	✘	✘	✘	✘	✘	✔	✔	✘	✔	✔	✘	✘	✔
Objective Function	**Revenue**	✘	✘	✘	✘	✘	✘	✔	✘	✘	✘	✘	✘	✘	✘	✘	✘	✘	✘	✘	✘	✘	✘	✔
	Gen. Cost	✔	✔	✔	✔	✔	✔	✔	✔	✔	✔	✔	✔	✔	✔	✔	✔	✔	✔	✔	✔	✔	✔	✔
	Storage Cost	✔	✔	✔	✔	✔	✔	✘	✔	✔	✔	✔	✘	✘	✘	✔	✔	✔	✔	✔	✔	✔	✔	✔
	Secu. Costs	✘	✘	✘	✘	✘	✘	✘	✘	✘	✘	✘	✘	✘	✘	✘	✘	✘	✘	✘	✘	✘	✘	✔
	PHEV cost	✘	✘	✘	✘	✘	✘	✘	✘	✘	✔	✘	✘	✘	✘	✘	✘	✘	✘	✘	✘	✘	✘	✔
	DRP costs	✘	✔	✘	✘	✘	✘	✔	✘	✔	✘	✘	✔	✔	✔	✘	✘	✘	✘	✘	✘	✘	✘	✔
	WT	✘	✔	✔	✘	✔	✔	✘	✔	✘	✔	✘	✔	✔	✘	✘	✔	✔	✔	✔	✘	✘	✘	✔
	PV	✔	✔	✔	✘	✔	✔	✘	✔	✘	✘	✘	✔	✔	✔	✘	✔	✔	✔	✔	✘	✘	✘	✔
DA-Market scheduling		✔	✔	✔	✔	✔	✔	✔	✔	✔	✔	✔	✔	✔	✔	✔	✔	✔	✔	✔	✔	✔	✔	✔
RT- Market scheduling		✘	✘	✘	✘	✘	✘	✘	✘	✘	✘	✘	✘	✘	✘	✔	✘	✘	✘	✔	✘	✘	✘	✔
Uncertainty Model	**PHEV**	✘	✘	✘	✘	✘	✘	✘	✘	✘	✘	✘	✘	✘	✘	✘	✘	✘	✘	✘	✘	✘	✘	✔
	DRP	✘	✘	✘	✘	✘	✘	✘	✘	✘	✘	✘	✘	✘	✘	✘	✘	✘	✘	✘	✘	✘	✘	✔
	DA Market price	✘	✔	✘	✘	✔	✔	✘	✘	✔	✘	✘	✘	✘	✘	✘	✘	✔	✘	✔	✘	✘	✘	✔
	RT Market price	✘	✘	✘	✘	✘	✘	✘	✘	✘	✘	✘	✘	✘	✘	✘	✘	✘	✘	✘	✘	✘	✘	✔
	Contingency	✘	✘	✘	✘	✘	✘	✘	✘	✘	✘	✘	✘	✘	✘	✘	✘	✘	✘	✘	✘	✘	✘	✔
	Loads	✘	✔	✘	✘	✔	✔	✘	✘	✔	✘	✘	✘	✘	✘	✘	✔	✔	✘	✔	✘	✘	✘	✔
	Inter. Electricity	✘	✔	✘	✘	✔	✔	✘	✘	✔	✘	✘	✘	✘	✘	✘	✔	✔	✘	✔	✘	✘	✘	✔

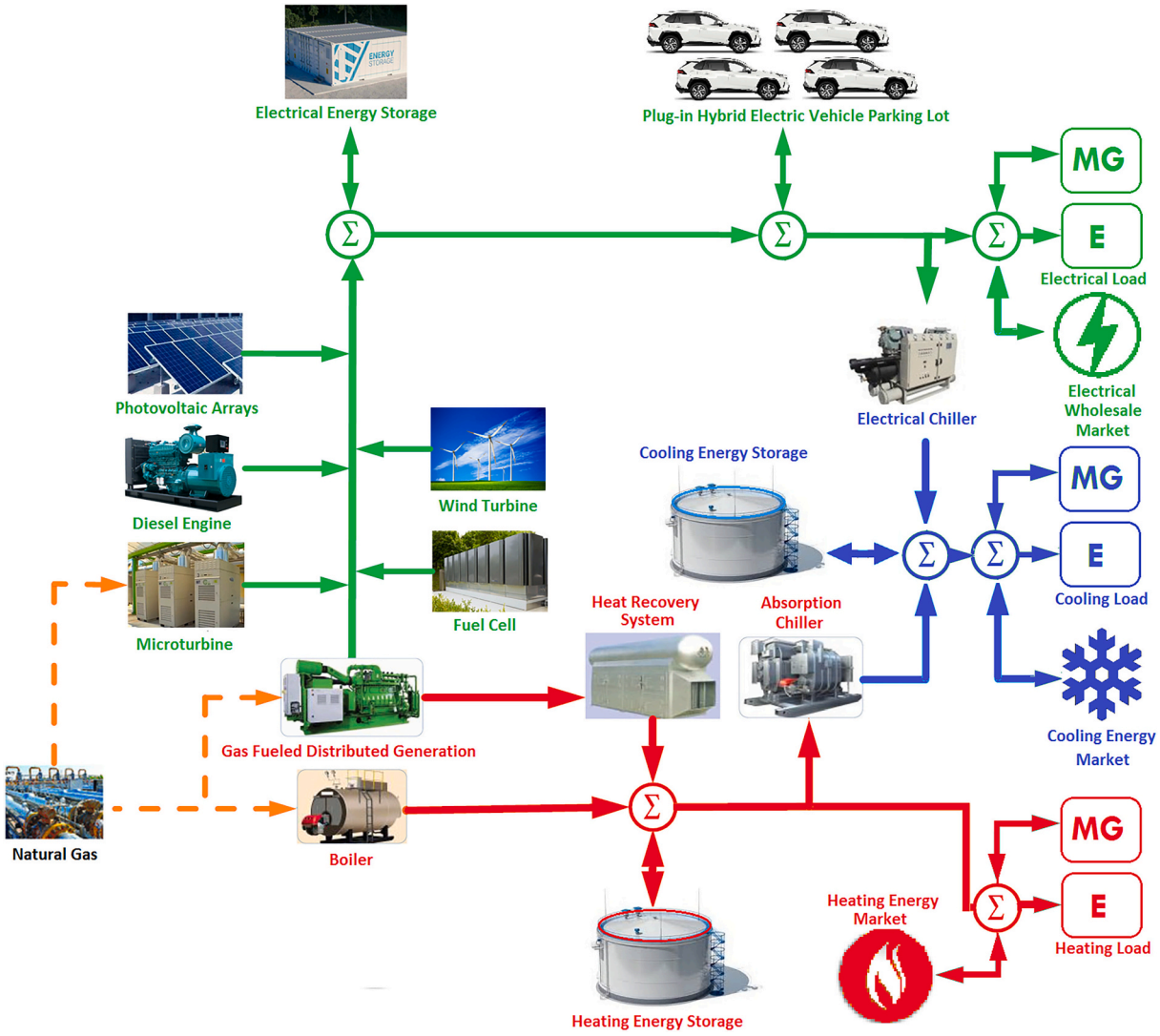

Fig. 1. Energy distribution system with its distributed energy resources.

determines the optimal operating strategy of the system for day-ahead and intra-day horizons. The objective functions include the operating cost, the cost of energy loss, the energy purchasing cost, and the emission pollutant cost. The method reduced the system costs by about 4.77% concerning the worst-case dispatch case. Ref. [18] studied the effectiveness of a collaborative energy management model to control heating, cooling, and electric loads. A Q-learning method was utilized to solve the problem. The model results were compared with the Genetic Algorithm (GA) and PSO results. The proposed method presented the lowest regulation cost, balanced power, and load fluctuations concerning the PSO and GA results. The model reduced the operating costs of the system by about 14.77% and 15.01% concerning the PSO and GA outputs, respectively. Refs. [17,18] did not assess the optimal scheduling of energy systems considering the heating and cooling markets.

Ref. [19] modeled the optimal scheduling of the system for day-ahead, intra-day, and real-time horizons using a two-stage robust optimization model. A CCG method was utilized to change the problem into a min–max-min problem. The results revealed that the intra-day problem reduced the costs of the worst-case scenario and the system reached the secure operating point in this case. Further, based on the proposed model, when the uncertain budget parameter of the system was increased to its maximum value, the increase in the system cost was the minimum. Ref. [20] proposed a robust energy management process for microgrids utilizing the Conditional Value-at-Risk (CVaR) model. An iterative sequential optimization process was used to solve the problem. The model utilized the linear decision rule to assess the uncertainty of energy flows. The method reduced the operating costs of the system by about 9.76% concerning the robust joint chance-constrained method. Refs. [19,20] did not consider the resilient operational scheduling of multi-carrier energy systems and switching of electrical switches and control valves.

Ref. [21] introduced a model to peak-load reduction and economic optimization. The linearization process was used to change the nonlinear problem into a MILP model. Then, an ε-constraint method was utilized to solve the problem. Finally, the Pareto optimal set was generated. The computation time was reduced by about 71.2%; meanwhile, the computational accuracy was improved by about 12.73%. The outputs of the MILP optimization process were compared with the outputs of GA, PSO, mutation PSO, and immune GA. The MILP had advantages in both computation time and accuracy in solving the problem. Ref. [22] evaluated an optimization model for a solar-driven CCHP system that determined the parameters and configuration of facilities. The sustainability indicator, annual total costs, and energy-saving ratio were utilized to assess the system's alternatives. Then, the multi-objective problem was modeled as a Pareto front optimization process. The case study was performed for a hotel and office building. The outputs presented that the annual costs of hotel and office buildings were reduced by about 7.69% and 7.33%, respectively. Refs. [21,22] did not

model the resilient operational scheduling of the energy system, switching of control valves, and real-time scheduling of the system.

1.2. Novel contribution

Based on the Literature Review subsection, Refs. [1–22] did not assess the energy transactions of multi-carrier MGs with the energy system considering the heating and cooling markets. Further, Refs. [1–22] did not optimize the electrical, heating, and cooling systems' topology considering the contingent condition of the system and the optimal commitment of MGs in this condition.

Thus, as shown in Table 1, a framework that considers the simultaneous optimal operation of multi-carrier MGs and their energy transactions with the energy system considering the heating and cooling markets, optimal switching of electrical switches, and heating and cooling control valves is less frequent in the recent literature.

An integrated model for incentive-based and price-based demand response processes that explores the impacts on the resilient operation of the energy system considering the switching of multi-carrier systems has been thus developed in this paper. The main novel contributions of this paper can be presented as:

- The proposed method considers the electrical, heating, and cooling energy transactions of the energy system with multi-carrier energy markets in the day-ahead and real-time horizons. Further, the multi-carrier energy transactions of MGs with the energy systems are modeled.
- The optimal switching of electrical switches and heating and cooling control valves in shock conditions is modeled.
- A resiliency index is proposed to assess the resiliency level of the energy system.
- The proposed solution process is decomposed into two-stage two-level optimization processes that optimize the energy system and MGs operational scheduling for day-ahead and real-time horizons.

2. Problem modeling and formulation

Fig. 1 shows the multi-carrier energy transactions of the energy distribution system with energy markets, microgrids, and system loads. The energy system has multiple electrical, heating, and cooling energy distributed energy resources, Plug-in Hybrid Electric Vehicles (PHEVs) parking lots, and energy storage facilities.

It is assumed that the optimal scheduling of distributed energy resources and load commitment is carried out by the Distribution System Operator (DSO) through smart grid infrastructure [23]. Further, the DSO utilizes two categories of demand response programs [24,25]: 1) incentive-based demand response programs, and 2) price-based demand response programs.

In the incentive-based demand response programs, the MGs gain profit based on their energy consumption reduction based on the multiplier of real-time energy market price [25]. Each MG submits a maximum value for its energy consumption reduction.

The price-based demand response programs consist of 1) fixed tariff, 2) Time-Of-Use (TOU) tariff, and 3) real-time tariff.

The energy consumption reduction of each consumer in TOU and real-time pricing processes is rewarded by the value of TOU and real-time market prices multiplied by the reduced energy consumption, respectively. However, the TOU and real-time tariff model do not utilize the submission process as defined for the incentive-based demand response process.

2.1. The wind turbine and photovoltaic arrays models

The Riley model is utilized to model wind speed. Eq. (1) presents the electrical power of a wind turbine:

$$P_w(v_{wind}) = \begin{cases} 0 & v_{wind} < v_{ci} \\ P_R \dfrac{(v_{wind} - v_{ci})}{(v_r - v_{ci})} & v_{ci} \le v_{wind} < v_r \\ P_R & v_r \le v_{wind} \le v_{co} \\ 0 & v_{wind} \ge v_{co} \end{cases} \quad (1)$$

where, v_{ci},v_r, v_{co}, and v_{wind} are cut-in wind velocity, nominal wind velocity, cut-out wind velocity, and wind velocity, respectively [23].

The maximum power output of photovoltaic arrays is written as (2) [23]:

$$\mathrm{P^{PV}} = A^{PV}.\eta.I.(1 - 0.005 \times (t_0 - 25)) \quad (2)$$

where, $A^{PV}, I, t_0, \eta$are the area of photovoltaic array, solar irradiation, outside air temperature, and photovoltaic array conversion efficiency, respectively.

The CCHPs, boilers, and energy storage facilities models are available in [23] and are not presented for the sack of space.

2.2. The electrical demand response process model

Based on the above description of the incentive-based process, the Incentive-Based Electrical Demand Response Program (IBEDRP) model considers that the aggregated electrical energy consumption reduction of each MG should be less than its submitted bid [25]. Based on this model, each microgrid can submit a load reduction bid for the next day-ahead operational scheduling process. Then, the DSO optimizes the energy system's day-ahead operational scheduling problem and determines the optimal values of load reduction bids of microgrids.

Thus, Eq. (3), Eq. (4), and Eq. (5) can be presented for IBEDRP of residential, commercial, and industrial microgrids, respectively.

$$AELRC(r,t) = SELRC(r,t).\alpha_{r,t}SELRC(r,t) \le SELRC_t^{\max} \quad (3)$$

where $AELRC(r,t), SELRC(r,t), \alpha_{r,t}, SELRC_t^{\max}$are the actual electrical load reduction of residential MG, the submitted value of electrical load reduction of residential MG, a pre-defined multiplier, and the maximum value of electrical load reduction of residential MG, respectively.

$$AELCC(c,t) = SELCC(c,t).\alpha_{c,t}SELCC(c,t) \le SELCC_t^{\max} \quad (4)$$

where $AELCC(c,t)$, $SERCC(c,t)$, $\alpha_{c,t}$, $SERCC_t^{\max}$are the actual electrical load reduction of commercial MG, the submitted value of electrical load reduction of commercial MG, a pre-defined multiplier, and the maximum value of electrical load reduction of commercial MG, respectively.

$$AELIC(i,t) = AELIC(i,t).\alpha_{i,t}SELIC(i,t) \le SELIC_t^{\max} \quad (5)$$

where $AELIC(i,t), SELIC(i,t), \alpha_{i,t}, SELIC_t^{\max}$are the actual electrical load reduction of industrial MG, the submitted value of electrical load reduction of industrial MG, a pre-defined multiplier, and the maximum value of electrical load reduction of industrial MG, respectively.

The energy management system of MGs can submit different values of electrical load reduction steps for the operational scheduling process.

2.3. The heating demand response process model

The Incentive-Based Heating Demand Response Program (IBHDRP) model formulation is the same as IBEDRP. Thus, Eq. (6), Eq. (7), and Eq. (8) can be presented for IBHDRP of residential, commercial, and industrial microgrids, respectively.

$$AHLRC(r,t) = SHLRC(r,t).\alpha'_{r,t}SHLRC(r,t) \le SHLRC_t^{\max} \quad (6)$$

where $AHLRC(r,t), SHLRC(r,t), \alpha'_{r,t}, SHLRC_t^{\max}$are the actual heating load reduction of residential MG, the submitted value of heating load

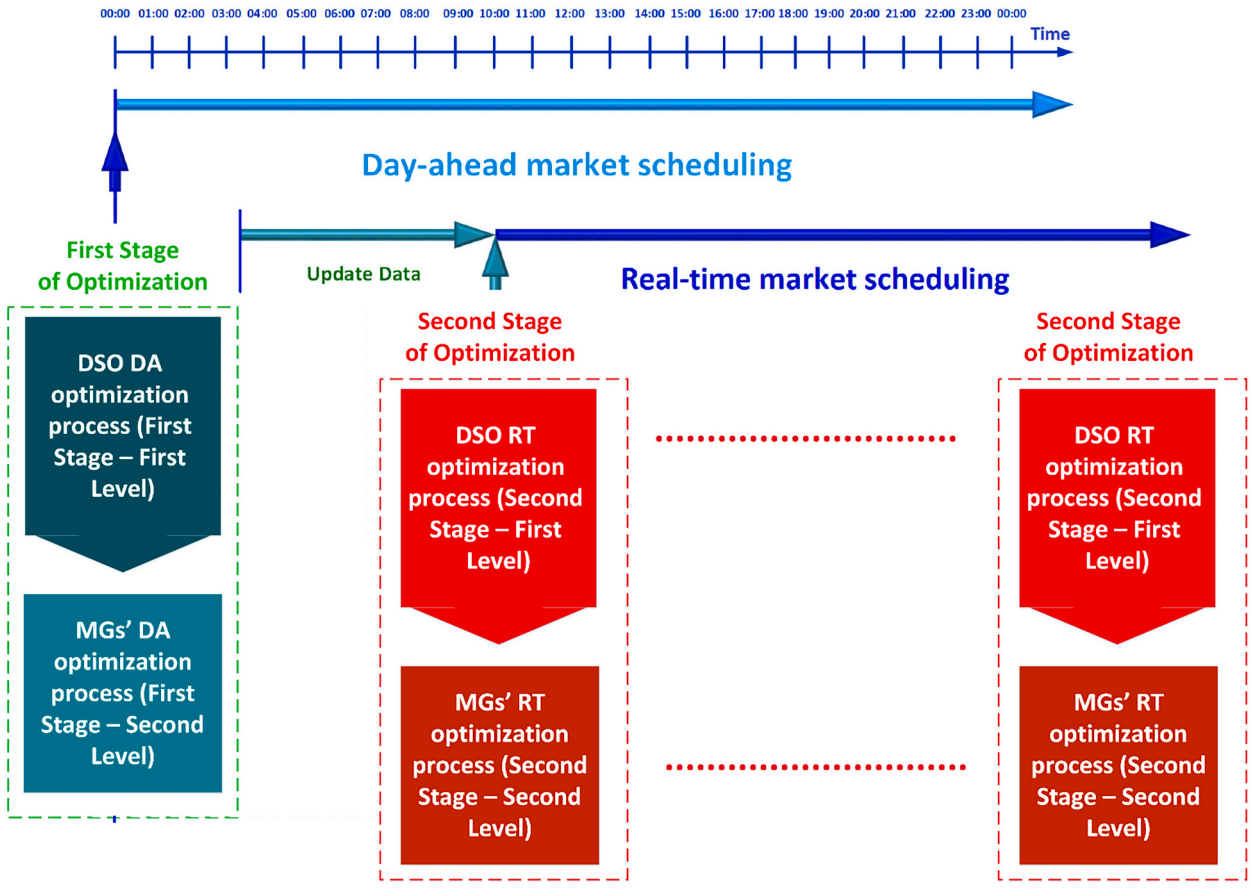

Fig. 2. The proposed framework for the optimization process.

reduction of residential MG, a pre-defined multiplier, and the maximum value of heating load reduction of residential MG, respectively.

$$AHLCC(c,t) = SHLCC(c,t).\alpha'_{c,t} SHLCC(c,t) \le SHLCC_t^{\max} \tag{7}$$

where $AHLCC(c,t)$, $SHRCC(c,t)$, $\alpha'_{c,t}$, $SHRCC_t^{\max}$ are the actual heating load reduction of commercial MG, the submitted value of heating load reduction of commercial MG, a pre-defined multiplier, and the maximum value of heating load reduction of commercial MG, respectively.

$$AHLIC(i,t) = AHLIC(i,t).\alpha'_{i,t} SHLIC(i,t) \le SHLIC_t^{\max} \tag{8}$$

where $AHLIC(i,t)$, $SHLIC(i,t)$, $\alpha'_{i,t}$, $SHLIC_t^{\max}$ are the actual heating load reduction of industrial MG, the submitted value of heating load reduction of industrial MG, a pre-defined multiplier, and the maximum value of heating load reduction of industrial MG, respectively.

2.4. The cooling demand response process model

The Incentive-Based Cooling Demand Response Program (IBCDRP) model formulation is the same as IBEDRP. Thus, Eq. (9), Eq. (10), and Eq. (11) can be presented for IBCDRP of residential, commercial, and industrial microgrids, respectively.

$$ACLRC(r,t) = SCLRC(r,t).\alpha''_{r,t} SCLRC(r,t) \le SCLRC_t^{\max} \tag{9}$$

where $ACLRC(r,t)$, $SCLRC(r,t)$, $\alpha''_{r,t}$, $SCLRC_t^{\max}$ are the actual cooling load reduction of residential consumers, the submitted value of cooling load reduction of residential consumers, a pre-defined multiplier, and the maximum value of cooling load reduction of residential consumers, respectively.

$$ACLCC(c,t) = SCLCC(c,t).\alpha''_{c,t} SCLCC(c,t) \le SCLCC_t^{\max} \tag{10}$$

where $ACLCC(c,t)$, $SCRCC(c,t)$, $\alpha''_{c,t}$, $SCRCC_t^{\max}$ are the actual cooling load reduction of commercial consumers, the submitted value of cooling load reduction of commercial consumers, a pre-defined multiplier, and the maximum value of cooling load reduction of commercial consumers, respectively.

$$ACLIC(i,t) = ACLIC(i,t).\alpha''_{i,t} SCLIC(i,t) \le SCLIC_t^{\max} \tag{11}$$

where $ACLIC(i,t)$, $SCLIC(i,t)$, $\alpha''_{i,t}$, $SCLIC_t^{\max}$ are the actual cooling load reduction of industrial consumers, the submitted value of cooling load reduction of industrial consumers, a pre-defined multiplier, and the maximum value of cooling load reduction of industrial consumers, respectively.

2.5. The objective function of DSO for day-ahead operational scheduling problem (First level of day-ahead optimization process)

As shown in Fig. 1, the DSO transacts electrical, heating, and cooling energy carriers with the wholesale electricity market, heating energy market, and cooling energy market, respectively in the day ahead and real-time horizons. The day-ahead optimization process determines the optimal scheduling of multi-carrier energy systems and MGs' DERs considering the forecasted values of multi-carrier energy consumptions, energy market prices, and intermittent energy generations. However, based on the stochastic behavior of intermittent energy generation and volatility of energy carriers' prices of electricity, heating, and cooling markets there are mismatches between the day-ahead optimal scheduling of DERs and the real-time operating conditions. Thus, a revised scheduling of energy systems and MGs' DERs should be carried out to

assess the impacts of energy generation and consumption mismatches. Hence, the optimization process should have two-stage optimization procedures, and these processes determine the optimal scheduling of the energy system and MGs in the day-ahead and real-time phases, respectively. The optimization framework is presented in Fig. 2. At the first stage optimization process, the DSO and MGs are optimizing their day-ahead objective functions in the first and second levels, respectively. Then, the real-time data are updated and in the second stage of optimization, the DSO and MGs optimize their real-time objective functions in the first and second levels, respectively. The optimization processes of the optimization framework are presented in the following subsections.

Based on Fig. 1 and Fig. 2, the DSO simultaneously transacts multi-carrier energy with microgrids and energy markets. Thus, the DSO can gain profit by selling energy carriers to MGs and energy markets. Thus, the distribution system operator should maximize the system reliability; meanwhile, minimizing the system operating costs. Thus, the objective function of the distribution system operator can be formulated as (12):

$$Min\ \mathbb{Z}_{DS}^{DA}(t) = \sum_{t=1}^{T} \mathbb{G}_{DS}^{DA}(t) + \sum_{t=1}^{T} \sum_{s=1}^{DSDAS} pr_s \cdot \mathbb{A}_{s\ DS}^{DA}(t) + \sum_{t=1}^{T} \sum_{k=1}^{DSRTS} pr_k \cdot \mathbb{Z}_{DS}^{RT} \quad (12)$$

where, $\mathbb{G}_{DS}^{DA}(t)$ consists of the following terms.

$$\begin{aligned}\mathbb{G}_{DS}^{DA}(t) = {} & \sum_{i=1}^{NDG} \left[P_{i\ DS}^{EDER}(t)\cdot\gamma_{i\ DS}(t)\cdot K_{i\ DS}(t) + SU_{i\ DS}(t)\cdot[K_{i\ DS}(t) - K_{i\ DS}(t-1)\,]\right] + \\ & \sum_{i'=1}^{NHDER} \left[H_{i'\ DS}^{HDER}(t)\cdot\gamma'_{i'DS}(t)\cdot K'_{i'DS}(t)\right] + \\ & \sum_{i''=1}^{NCDER} \left[R_{i''\ DS}^{CDER}(t)\cdot\gamma''_{i''DS}(t)\cdot K''_{i''DS}(t)\right] + \\ & \sum_{j=1}^{J} C_{j\ MG}^{IBEDR\_DA}(t) + \sum_{j'=1}^{J'} C_{j'MG}^{IBHDR\_DA}(t) + \sum_{j''=1}^{J''} C_{j''MG}^{IBCDR\_DA}(t) + \sum_{g=1}^{G} C_{g\ MG}^{PBEDR\_DA}(t) + \\ & \sum_{g'=1}^{G'} C_{g'MG}^{PBHDR\_DA}(t) + \sum_{g'=1}^{G''} C_{g'MG}^{PBCDR\_DA}(t) + C_{DS}^{PHEVPL\_DA}(t) - B_{DS}^{PHEVPL\_DA}(t) + \\ & C_{DS}^{E\_IMPORT\_DA}(t) - B_{DS}^{E\_EXPORT\_DA}(t) + C_{DS}^{H\_IMPORT\_DA}(t) - B_{DS}^{H\_EXPORT\_DA}(t) + \\ & C_{DS}^{C\_IMPORT\_DA}(t) - B_{DS}^{C\_EXPORT\_DA}(t)\end{aligned} \quad (13)$$

Eq. (13) consists of the operating costs of DSO electrical distributed energy resources ($P_{i\ DS}^{EDER}(t)\cdot\gamma_{i\ DS}(t)\cdot K_{i\ DS}(t)$), DSO's start-up costs ($SU_{i\ DS}(t)\cdot[K_{i\ DS}(t) - K_{i\ DS}(t-1)\,]$), operating costs of DSO heating energy distributed energy resources ($H_{i'DS}^{HDER}(t)\cdot\gamma'_{i'DS}(t)\cdot K'_{i'DS}(t)$), operating costs of DSO cooling energy resources ($R_{i''DS}^{CDER}(t)\cdot\gamma''_{i''DS}(t)\cdot K''_{i''DS}(t)$), the costs of IBEDRP paid to MGs ($C_{j\ MG}^{IBEDR\_DA}(t)$), the costs of IBHDRP paid to MGs ($C_{j'MG}^{IBHDR\_DA}(t)$), the costs of IBCDRP paid to MGs ($C_{j''MG}^{IBCDR\_DA}(t)$), the costs of Price-Based Electrical Demand Response Program (PBEDRP) paid to MGs ($C_{g\ MG}^{PBEDR\_DA}(t)$), the costs of Price-Based Heating Demand Response Program (PBHDRP) paid to MGs ($C_{g'MG}^{PBHDR\_DA}(t)$), the costs of Price-Based Cooling Demand Response Program (PBCDRP) paid to MGs ($C_{g''MG}^{PBCDR\_DA}(t)$), costs of electrical energy purchased from wholesale electricity market ($C_{DS}^{IMPORT\_DA}(t)$), costs of electrical energy purchased from PHEV parking lots ($C_{DS}^{PHEVPL\_DA}(t)$), and benefits of electrical energy sold to PHEV parking lots ($B_{DS}^{PHEVPL\_DA}(t)$).

$C_{DS}^{E\_IMPORT\_DA}(t)$, $B_{DS}^{E_EXPORT_DA}(t)$are the DSO's imported electricity costs and exported electricity benefits, respectively. $C_{DS}^{H\_IMPORT\_DA}(t)$, $B_{DS}^{H_EXPORT_DA}(t)$are the DSO's imported heating energy costs and exported heating energy benefits, respectively. $C_{DS}^{C\_IMPORT\_DA}(t)$, $B_{DS}^{C_EXPORT_DA}(t)$are the DSO's imported cooling energy costs and exported cooling energy benefits, respectively.

Where, $P_{i\ DS}(t), \gamma_{i\ DS}(t), K_{i\ DS}(t)$ are DSO's generated power of distributed energy resources, cost of energy generation, and binary decision variable of DSO's DER commitment, respectively.

The $\mathbb{A}_{s\ DS}^{DA}(t)$ is decomposed into the following terms.

$$\begin{aligned}\mathbb{A}_{s\ DS}^{DA}(t) = {} & \sum_{i=1}^{NIDG} C_{(i,s)\ DS}^{IDG}(t) + \sum_{g=1}^{G} VC_{(g,s)\ MG}^{PBEDR\_DA}(t) + \sum_{g'=1}^{G'} VC_{(g',s)\ MG}^{PBHDR\_DA}(t) + \sum_{g''=1}^{G''} VC_{(g'',s)\ MG}^{PBCDR\_DA}(t) + \\ & EENSC_{S\ DS}(t) + HENSC_{S\ DS}(t) + CENSC_{S\ DS}(t)\end{aligned} \quad (14)$$

Eq. (14) consists of the operating costs of DSO's intermittent electricity facilities ($C_{(i,s)\ DS}^{IDG}(t)$), the variable costs of PBEDRP paid to MGs ($VC_{MG}^{PBEDR\_DA}(t)$), the variable costs of PBHDRP paid to MGs ($VC_{MG}^{PBHDR\_DA}(t)$), the s variable costs of PBCDRP paid to MGs ($VC_{MG}^{PBCDR\_DA}(t)$), the electrical energy not supplied costs ($EENSC_{S\ DS}(t)$), the heating energy not supplied costs ($HENSC_{S\ DS}(t)$), the cooling energy not supplied costs ($CENSC_{S\ DS}(t)$).

The proposed second objective function can be presented as (15):

$$\mathbb{B}_{DS}^{DA}(t) = TENP_{DG\ DS}(t) + TENP_{Market\ DS}(t) \quad (15)$$

Eq. (15) consists of the volume of environmental pollution of DSO's distributed generation units and the fossil-fuelled electricity generation of wholesale market units, respectively. Where, $TENP_{DG\ DS}(t)$ and $TENP_{Market}(t)$ are formulated as Eq. (16) and Eq. (17), respectively.

$$TENP_{DG\ DS}(t) = \sum_{i=1}^{NDG}\left[ENP^{DG}_{CO2\ DS}(t) + ENP^{DG}_{SO2\ DS}(t) + ENP^{DG}_{NOx\ DS}(t)\right)\cdot P^{DG}_{DS}(t)\Big] \tag{16}$$

where, $ENP^{DG}_{CO2}(t), ENP^{DG}_{SO2}(t), ENP^{DG}_{NOx}(t)$are the volumes of CO_2, SO_2, and NOx pollution of distributed generation units, respectively.

$$TENP_{Market}(t) = ENP^{Market}_{CO2\ Market}(t) + ENP^{Market}_{SO2\ Market}(t) + ENP^{Market}_{NOx\ Market}(t) \tag{17}$$

where, $ENP^{Market}_{CO2\ Market}(t), ENP^{Market}_{SO2\ Market}(t), ENP^{Market}_{NOx\ Market}(t)$are the volumes of CO_2, SO_2, and NOx pollution of wholesale market generation units, respectively.

The $\mathbb{Z}^{RT}_{DS}$ is the objective function of DSO's real-time optimization problem.

The proposed objective function has the following constraints.

A. Electric power balance constraint

The electrical power balance constraint should be satisfied for any simulation interval as (18):

$$\begin{aligned}&\sum_{i=1}^{NDG} P^{EDER}_{i,s\ DS}(t) \mp P^{E\_Market}_{s\ DS}(t) + P^{CCHP}_{s\ DS}(t) \mp P^{ESS}_{s\ DS}(t) \mp P^{PHEVPL}_{s\ DS}(t) = \\ &\sum_{m=1}^{NEL} P^{L}_{m,s\ DS}(t) - \sum_{a=1}^{NRMG} AELRC_{a,s\ MG}(t) - \sum_{a'=1}^{NCMG} AELCC_{a',s\ MG}(t) - \\ &\sum_{a''=1}^{NIMG} AELIC_{a'',s\ MG}(t) - \sum_{b=1}^{NEIBDR} P^{PBDR}_{b,s\ DS}(t) + P^{CCH}_{s\ DS}(t)\end{aligned} \tag{18}$$

Eq. (18) presents that the aggregated generated electrical power of DSO's distributed generation units ($P^{EDER}_{i,s\ DS}(t)$), the exported (imported) power to (from) electricity market ($P^{E\_Market}_{s\ DS}(t)$), generated power of CCHP ($P^{CCHP}_{s\ DS}(t)$), transacted electrical power with electrical energy storages ($P^{ESS}_{s\ DS}(t)$), and transacted electrical power with PHEV parking lots ($P^{PHEVPL}_{s\ DS}$) should be equal to the aggregated active power of loads $P^{L}_{m,s\ DS}(t)$, residential MG load reduction $AELRC_{a,s\ MG}(t)$, commercial MG load reduction ($AELCC_{a',s\ MG}(t)$), industrial MG load reduction ($AELIC_{a'',s\ MG}(t)$), electrical loads participating in price-based demand response programs ($P^{PBDR}_{b,s\ DS}(t)$), and the electricity consumption of compressed chiller ($P^{CCH}_{s\ DS}(t)$).

B. Heating power balance constraint

The heating power balance constraint of DSO should be satisfied for any simulation interval as (19):

$$\begin{aligned}&H^{CCHP}_{s\ DS}(t) \mp H^{H\_Market}_{s\ DS}(t) + H^{Boiler}_{s\ DS}(t) \mp H^{TES}_{s\ DS}(t) = \\ &\sum_{m=1}^{NHL} H^{L}_{m,s\ DS}(t) - \sum_{a=1}^{NRMG} AHLRC_{a,s\ MG}(t) - \sum_{a'=1}^{NCMG} AHLCC_{a',s\ MG}(t) - \\ &\sum_{a''=1}^{NIMG} AHLIC_{a',s\ MG}(t) - \sum_{b=1}^{NHIBDR} H^{PBDR}_{b,s\ DS}(t) + H^{ACH}_{s\ DS}(t)\end{aligned} \tag{19}$$

Eq. (19) presents that the aggregated generated heating power of DSO's CCHP units ($H^{CCHP}_{s\ DS}(t)$), the exported (imported) power to (from) heating energy market ($H^{H\_Market}_{s\ DS}(t)$), generated heating power of the boiler ($H^{Boiler}_{s\ DS}(t)$), and the heating power transactions of the thermal energy storages ($H^{TES}_{s\ DS}(t)$) should be equal to the aggregated heating power of loads ($H^{L}_{m,s\ DS}(t)$), residential MG heating load reduction ($AHLRC_{a,s\ MG}(t)$), commercial MG heating load reduction ($AHLCC_{a',s\ MG}(t)$), industrial MG heating load reduction ($AHLIC_{a'',s\ MG}(t)$), PBHDRP heating loads ($H^{PBDR}_{b,s\ DS}(t)$), and the heating energy consumption of absorption chiller ($H^{ACH}_{s\ DS}(t)$).

C. Cooling power balance constraint

The cooling power balance constraint of DSO should be satisfied for any simulation interval as Eq. (20):

$$\begin{aligned}&R^{CCHP}_{s\ DS}(t) \mp R^{C\_Market}_{s\ DS}(t) + R^{ACH}_{s\ DS}(t) + R^{CCH}_{s\ DS}(t) = \\ &\sum_{m=1}^{NCL} R^{L}_{m,s\ DS}(t) - \sum_{a=1}^{NRMG} ACLRC_{a,s\ MG}(t) - \sum_{a'=1}^{NCMG} ACLCC_{a',s\ MG}(t) \\ &- \sum_{a''=1}^{NIMG} ACLIC_{a'',s\ MG}(t) - \sum_{b=1}^{NCIBDR} R^{PBDR}_{b,s\ DS}(t)\end{aligned} \tag{20}$$

Eq. (20) presents that the aggregated generated cooling power of DSO's CCHP units ($R^{CCHP}_{s\ DS}(t)$), the exported (imported) power to (from) cooling energy market ($R^{C\_Market}_{s\ DS}(t)$), and generated cooling power of absorption chillers ($R^{ACH}_{s\ DS}(t)$) and compressed chillers ($R^{CCH}_{s\ DS}(t)$) should be equal to the aggregated cooling power of DSO's loads ($R^{L}_{m,s\ DS}(t)$), residential MG cooling load reduction ($ACLRC_{a,s\ MG}(t)$), commercial MG cooling load reduction ($ACLCC_{a',s\ MG}(t)$), industrial MG cooling load reduction ($ACLIC_{a'',s\ MG}(t)$), and PBCDRP cooling loads ($R^{PBDR}_{b,s\ DS}(t)$).

The AC load flow constraints for the electrical system, the constraints of facilities' maximum capacity, charge, and discharge constraints, and mass balance constraints should be considered for each of the simulation intervals and are not presented for the sake of space.

2.6. The objective function of MGs for day-ahead operational scheduling problem (Second level of day-ahead optimization process)

As shown in Fig. 1, the MGs transact energy carriers with the DSO. The MG's operator should minimize the operating costs of MG; meanwhile, maximizing the energy transactions and demand response programs' contributions profits. Thus, the proposed day-ahead objective functions of MGs consist of the following terms: 1) The fixed and start-up costs of operating costs of MGs' distributed generation units, demand response program benefits, and costs (benefits) of imported/exported energy from/to energy system, 2) The operating costs of MG's intermittent electricity generation considering uncertainties, the variable operating costs of MGs' distributed generation units, the load commitment benefits, and energy not supplied costs, 3) the costs of environmental pollutions, 4) and the expected value of the real-time objective function.

The objective function can be presented as (21):

$$\begin{aligned}Min\ F^{DA}_{MG}(x) = &\sum_{t=1}^{T} \mathfrak{M}^{DA}_{MG}(t) + \sum_{t=1}^{T}\sum_{s=1}^{MGDAS} pr_s\cdot\mathfrak{I}^{DA}_{s\ MG}(t) + \sum_{t=1}^{T} \mathbb{S}^{DA}_{MG}(t) + \sum_{t=1}^{T} \\ &\times \sum_{k=1}^{MGRTS} pr_k\cdot F^{RT}_{MG}\end{aligned} \tag{21}$$

where, $\mathfrak{M}^{DA}_{MG}(t)$ is presented as (22):

$$
\begin{aligned}
\mathfrak{M}_{MG}^{DA}(t) = & \sum_{i=1}^{NDG'} \left[P_{i\ MG}^{DG}(t)\cdot\gamma_{i\ MG}(t)\cdot K_{i\ MG}(t)\right]+ \\
& \sum_{i'=1}^{NHRMG} \left[H_{i\ MG}^{HDER}(t)\cdot\gamma'_{i'MG}(t)\cdot K'_{i'MG}(t)\right]+ \\
& \sum_{i''=1}^{NCRMG} \left[R_{i\ MG}^{CDER}(t)\cdot\gamma''_{i''MG}(t)\cdot K''_{i''MG}(t)\right]+ \\
& \sum_{j=1}^{J} B_{j\ MG}^{IBEDR\_DA}(t) + \sum_{j'=1}^{J'} B_{j'MG}^{IBHDR\_DA}(t) + \sum_{j''=1}^{J''} B_{j''MG}^{IBCDR\_DA}(t) + \sum_{g=1}^{G} B_{g\ MG}^{PBEDR\_DA}(t)+ \\
& \sum_{g'=1}^{G'} B_{g'MG}^{PBHDR\_DA}(t) + \sum_{g''=1}^{G''} B_{g''MG}^{PBCDR\_DA}(t) + C_{MG}^{IMPORT\_DA}(t) - B_{MG}^{EXPORT\_DA}(t)
\end{aligned}
\tag{22}
$$

Eq. (21) consists of the MG's operating costs of electrical distributed generation units ($P_{i\ MG}^{DG}(t)\cdot\gamma_{i\ MG}(t)\cdot K_{i\ MG}(t)$), operating costs of MG's heating energy distributed energy resources ($H_{i'MG}^{HDER}(t)\cdot\gamma'_{i'MG}(t)\cdot K'_{i'MG}(t)$), operating costs of MG's cooling energy resources ($R_{i''MG}^{CDER}(t)\cdot\gamma''_{i''MG}(t)\cdot K''_{i''MG}(t)$), the benefits of IBEDRP ($B_{j\ MG}^{IBEDR\_DA}(t)$), the benefits of IBHDRP ($B_{j'MG}^{IBHDR\_DA}(t)$), the benefits of IBCDRP ($B_{j''MG}^{IBCDR\_DA}(t)$), the benefits of PBEDRP ($B_{g\ MG}^{PBEDR\_DA}(t)$), the benefits of PBHDRP ($B_{g'MG}^{PBHDR\_DA}(t)$), the benefits of PBCDRP ($B_{g''MG}^{PBCDR\_DA}(t)$), costs of electrical energy purchased from the energy system($C_{MG}^{IMPORT\_DA}(t)$), and benefit of electrical, heating, and cooling energy sold to the energy system ($B_{MG}^{EXPORT\_DA}(t)$).

Where, $P_{i\ MG}(t), \gamma_{i\ MG}(t), K_{i\ MG}(t)$ are generated power of MG distributed generation unit, cost of electrical energy generation of MG, and binary decision variable of unit commitment of MG facilities, respectively.

The $\mathfrak{N}_{s\ MG}^{DA}(t)$ term consists of Eq. (23) terms.

$$
\begin{aligned}
\mathfrak{N}_{s\ MG}^{DA}(t) = & \sum_{i=1}^{NIDG'} C_{(i,s)\ MG}^{IDG}(t) + \sum_{j=1}^{J} Penalty_{(j,s)\ MG}^{IBEDR\_DA}(t)+ \\
& \sum_{j'=1}^{J'} Penalty_{(j',s)\ MG}^{IBHDR\_DA}(t) + \sum_{j''=1}^{J''} Penalty_{(j'',s)\ MG}^{IBCDR\_DA}(t)+ \\
& EENSC_{S\ MG}(t) + HENSC_{S\ MG}(t) + CENSC_{S\ MG}(t)
\end{aligned}
\tag{23}
$$

Eq. (23) consists of the operating costs of MG's intermittent electricity facilities ($C_{(i,s)\ MG}^{IDG}(t)$), the penalty costs of MG's IBEDRP ($Penalty_{(j,s)\ MG}^{IBEDR\_DA}(t)$), the penalty costs of MG's IBHDRP ($Penalty_{(j',s)\ MG}^{IBHDR\_DA}(t)$), the penalty costs of MG's IBCDRP ($Penalty_{(j'',s)\ MG}^{IBCDR\_DA}(t)$), the electrical energy not supplied costs of MG ($EENSC_{S\ MG}(t)$), the heating energy not supplied costs of MG ($HENSC_{S\ MG}(t)$), the cooling energy not supplied costs of MG ($CENSC_{S\ MG}(t)$).

The third term of the objective function of Eq. (21) can be presented as (24):

$$
\mathbb{S}_{MG}^{DA}(t) = TENP_{DG\ MG}(t) \tag{24}
$$

Eq. (24) consists of the volume of environmental pollution of distributed generation units of MG, which can be formulated as (25):

$$
TENP_{DG\ MG}(t) = \sum_{i=1}^{NDG'} \left[ENP_{CO2\ MG}^{DG}(t) + ENP_{SO2\ MG}^{DG}(t) + ENP_{NOx\ MG}^{DG}(t)\right)\cdot P_{MG}^{DG}(t)\Big] \tag{25}
$$

where, $ENP_{CO2}^{DG}(t), ENP_{SO2}^{DG}(t), ENP_{NOx}^{DG}(t)$are the volumes of CO_2, SO_2, and NOx pollution of MG's distributed generation unit, respectively.

The F_{MG}^{RT} is the objective function of MG's real-time optimization problem.

The proposed objective function has the following constraints.

A. Electric power balance constraint

The electrical power balance constraint of MG should be satisfied for any simulation interval, which can be formulated as (26):

$$
\begin{aligned}
& \sum_{i=1}^{NDG'} P_{i,s\ MG}^{DG}(t) \mp P_{s\ MG}^{DSO}(t) + P_{s\ MG}^{CCHP}(t) \mp P_{s\ MG}^{ESS}(t) \mp P_{s\ MG}^{PHEV}(t) = \\
& \qquad \sum_{m=1}^{NEL'} P_{m,s\ MG}^{L}(t) - P_{b,s\ MG}^{PBDR}(t) + P_{s\ MG}^{CCH}(t)
\end{aligned}
\tag{26}
$$

Eq. (26) presents that the aggregated generated electrical power of distributed generation units of MG ($P_{i,s\ MG}^{DG}$), the exported (imported) power to (from) electrical energy system($P_{s\ MG}^{DSO}(t)$), generated electrical power of MG's CCHP ($P_{s\ MG}^{CCHP}(t)$), transacted electrical power with electrical storages ($P_{s\ MG}^{ESS}(t)$), and transacted electrical power with PHEVs' parking lots ($P_{s\ MG}^{PHEV}(t)$) should be equal to the aggregated active power of MG's loads ($P_{m,s\ MG}^{L}$), price-based demand response programs MG's electrical loads ($P_{b,s\ MG}^{PBDR}(t)$), and the electricity consumption of compressed chiller ($P_{s\ MG}^{CCH}(t)$).

B. Heating power balance constraint

The heating power balance constraint should be satisfied for any simulation interval, which can be formulated as (27):

$$
\begin{aligned}
& H_{s\ MG}^{CCHP}(t) + H_{s\ MG}^{Boiler}(t) = \\
& \sum_{m=1}^{NHL'} H_{m,s\ MG}^{L}(t) - H_{b,s\ MG}^{PBDR}(t) + H_{s\ MG}^{ACH}(t)
\end{aligned}
\tag{27}
$$

Eq. (27) presents that the aggregated generated heating power of MG's CCHP units ($H_{s\ MG}^{CCHP}(t)$), and generated heating power of MG's boiler ($H_{s\ MG}^{Boiler}(t)$) should be equal to the aggregated MG's heating power of loads ($H_{m,s\ MG}^{L}(t)$), MG's PBHDRPs heating loads ($H_{b,s\ MG}^{PBDR}(t)$), and the MG's heating energy consumption of absorption chiller ($H_{s\ MG}^{ACH}(t)$).

C. Cooling power balance constraint

The cooling power balance constraint of MG should be satisfied for any simulation interval, which can be presented as (28):

$$
\begin{aligned}
& R_{s\ MG}^{CCHP}(t) + R_{s\ MG}^{ACH}(t) + R_{s\ MG}^{CCH}(t) = \\
& \sum_{m=1}^{NCL'} R_{m,s\ MG}^{L}(t) - R_{b,s\ MG}^{PBDR}(t)
\end{aligned}
\tag{28}
$$

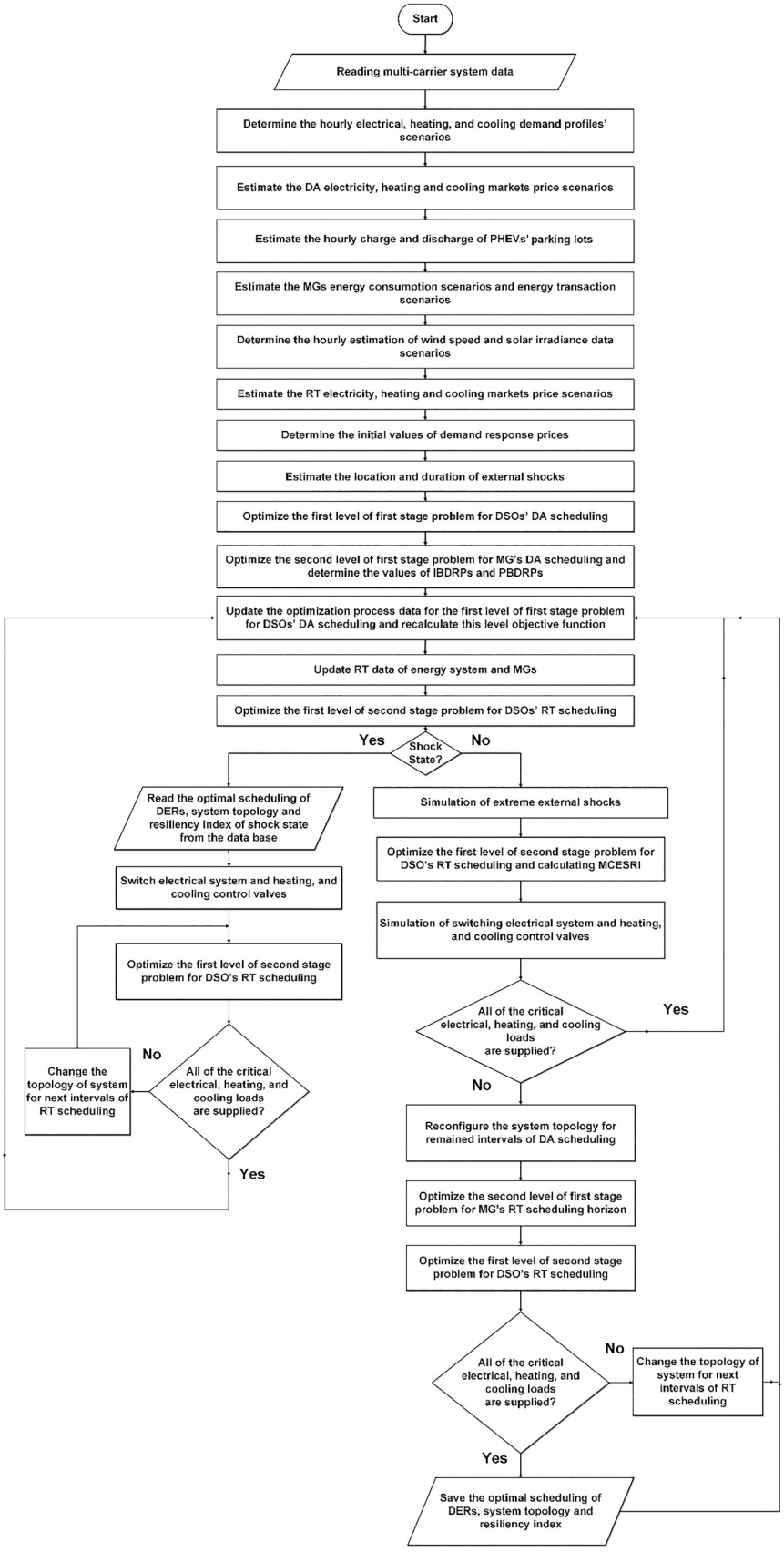

Fig. 3. The flowchart of the proposed procedure.

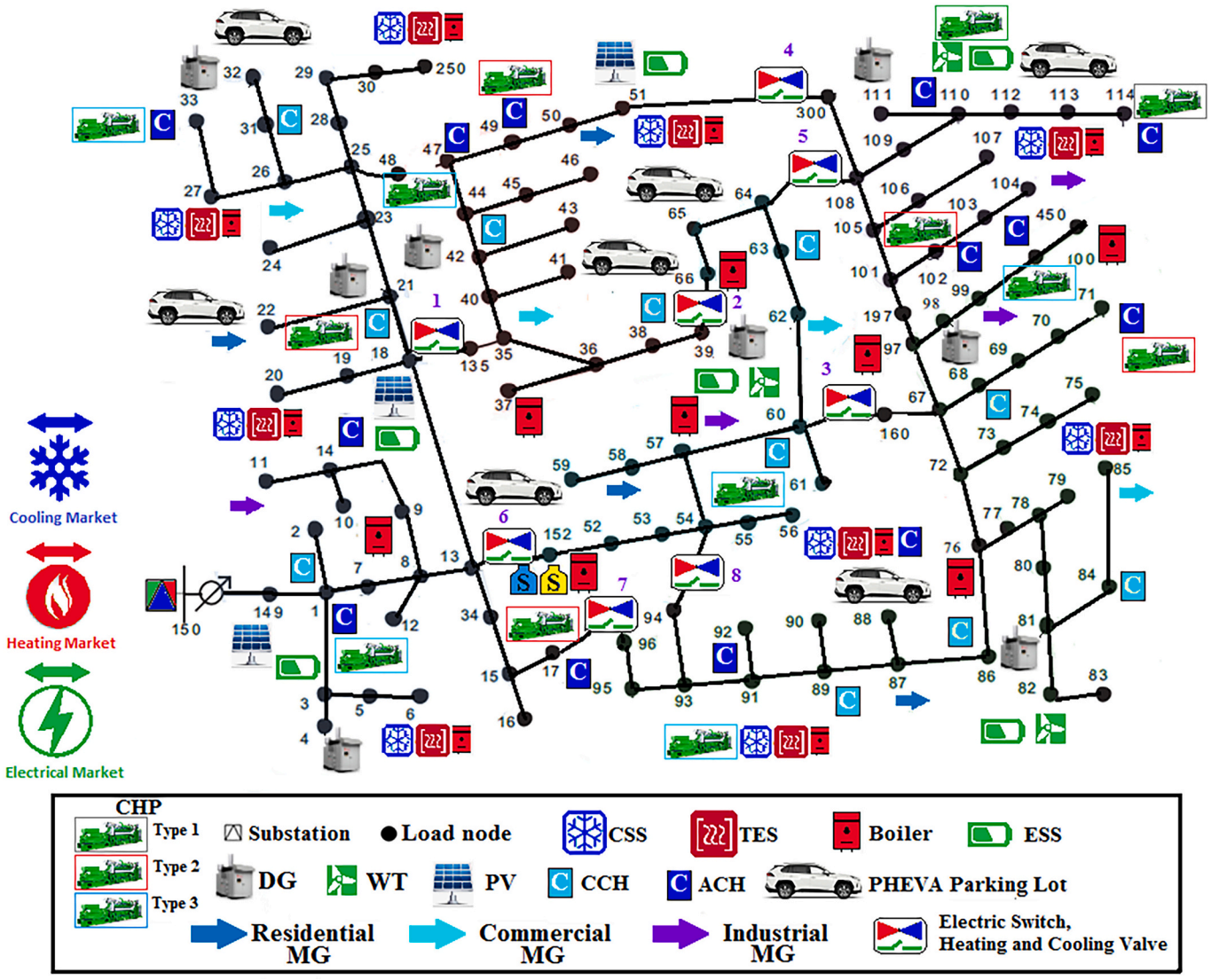

Fig. 4. The topology of the modified 123-bus test system.

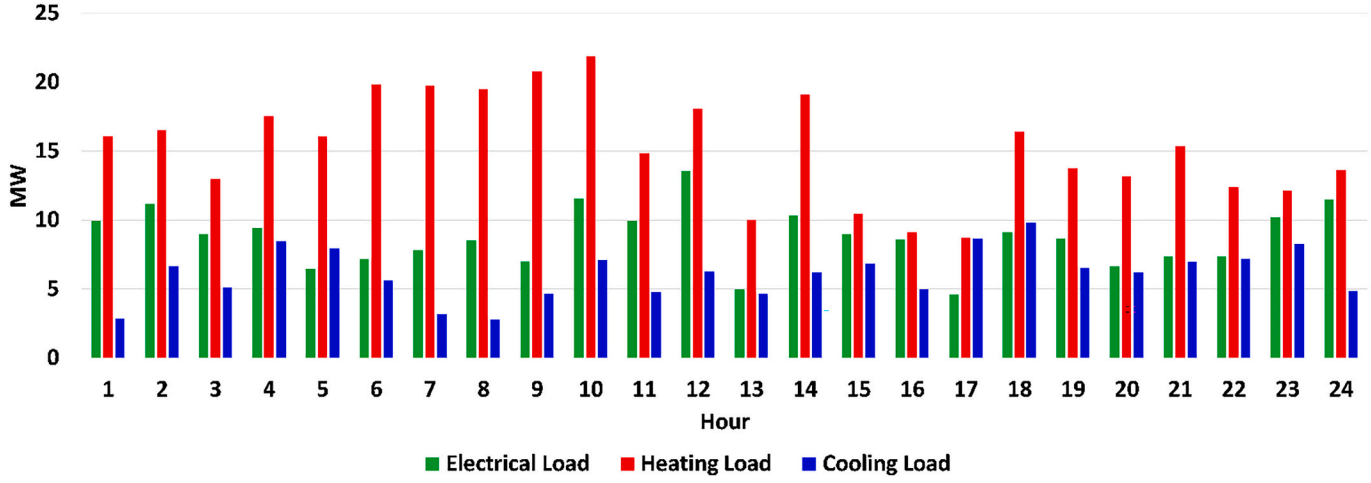

Fig. 5. The estimated energy consumption of electrical, heating, and cooling loads of the 123-bus system.

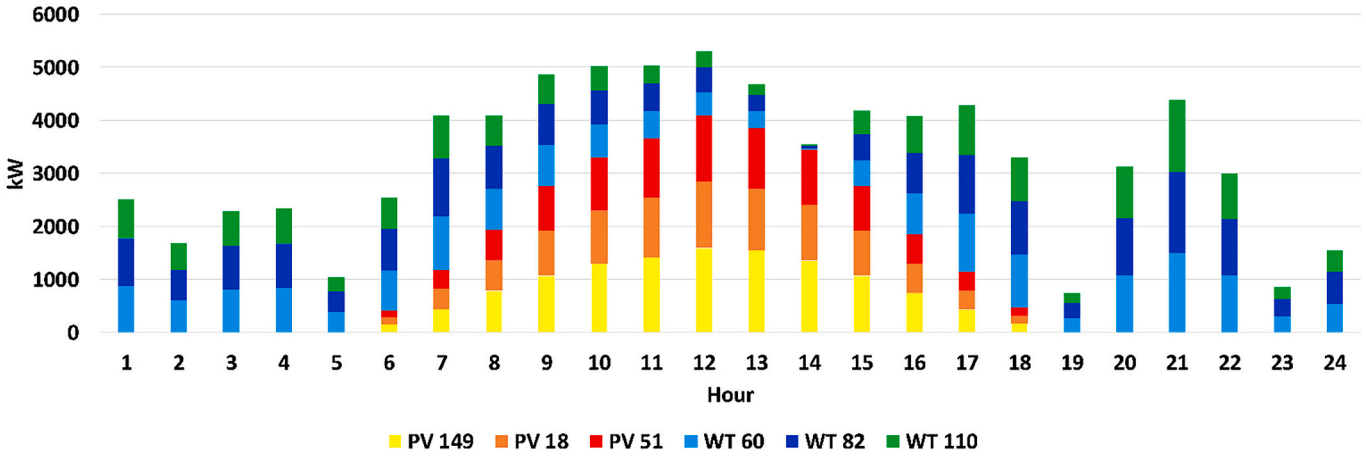

Fig. 6. The estimated values of energy generation of wind turbines and photovoltaic arrays of 123-bus system.

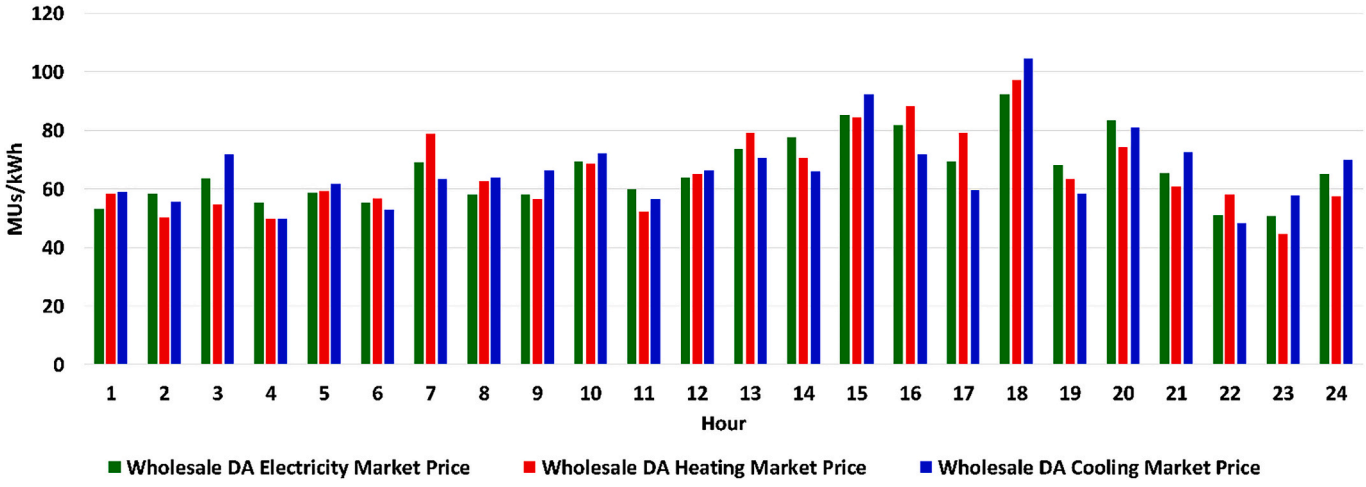

Fig. 7. The estimated price of day-ahead electrical, heating, and cooling markets.

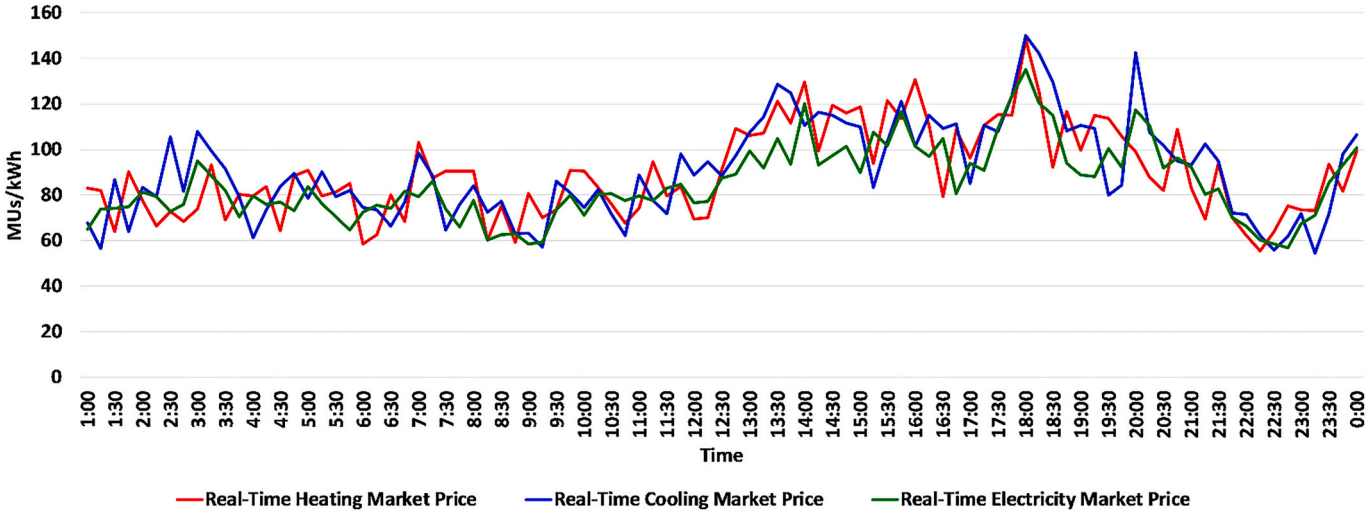

Fig. 8. The estimated price of real-time electrical, heating, and cooling markets.

Eq. (28) presents that the aggregated generated cooling power of MG's CCHP units ($R^{CCHP}_{s\ MG}(t)$), and generated cooling power of absorption chillers ($R^{ACH}_{s\ MG}(t)$) and compressed chillers ($R^{CCH}_{s\ MG}(t)$) should be equal to the aggregated MG's cooling power of loads ($R^{L}_{m,s\ MG}$), and MG's PBCDRPs cooling loads ($R^{PBDR}_{b,s\ MG}(t)$.

The AC load flow constraints for the electrical system, the constraints of facilities' maximum capacity, charge, and discharge constraints, and mass balance constraints should be considered for each of the simulation

intervals and are not presented for the sake of space.

2.7. The objective function of DSO for the real-time operational scheduling problem (First level of real-time optimization process)

As shown in Fig. 2, the energy system and MGs data are updated for real-time operational scheduling. The DSO should minimize the operating costs; meanwhile, maximizing the benefit of energy transactions with the electrical, heating, and cooling markets. Further, the DSO should minimize the unserved load considering the shock conditions. Finally, the DSO should optimize the status of electrical switches and heating and cooling valves. Thus, the distribution system operator's objective function for the real-time operating conditions can be formulated as (29):

$$\begin{aligned} Min\ \mathbb{Z}^{RT}_{DS}(x) = \sum_{k=1}^{NRTSS} W_1 \cdot \Bigg(& \mathbb{G}^{RT}_{k\ DS}(t) + \mathbb{A}^{RT}_{k\ DS}(t) + \mathbb{B}^{RT}_{k\ DS}(t) + \\ & W_2 \cdot \left[\sum_{k'=1}^{NEL} (1 - P_{0\ k'}) + \sum_{k''=1}^{NHL} (1 - H_{0\ k''}) + \sum_{k'''=1}^{NCL} (1 - R_{0\ k'''}) \right] + \\ & W_3 \cdot \left[\sum_{j=1}^{NNCSW} X^{EL}_{j} + \sum_{j'=1}^{NNCHV} X^{HCV}_{j'} + \sum_{j''=1}^{NNCCV} X^{CCV}_{j''} \right] \\ & \forall \Omega \in \{\text{Normal and Contingent Conditions}\} \end{aligned} \tag{29}$$

Eq. (29) decomposed into DSO's costs $\sum_{k=1}^{NRTST} W_1 \cdot \left(\mathbb{G}^{RT}_{k\ DS}(t) + \mathbb{A}^{RT}_{k\ DS}(t) + \mathbb{B}^{RT}_{k\ DS}(t) \right)$, the unserved loads of electrical, heating, and cooling systems $\left[\sum_{k'=1}^{NEL} (1 - P_{0\ k'}) + \sum_{k''=1}^{NHL} (1 - H_{0\ k''}) + \sum_{k'''=1}^{NCL} (1 - R_{0\ k'''}) \right]$, and the switching of electrical switches, heating, and cooling system control valves $\left[\sum_{j=1}^{NNCSW} X^{EL}_{j} + \sum_{j'=1}^{NNCHV} X^{HCV}_{j'} + \sum_{j''=1}^{NNCCV} X^{CCV}_{j''} \right]$.

It is assumed that the DSO can switch the boundary lines' switches and heating and cooling valves in normal and shock conditions to perform preventive/corrective actions.

Eq. (30) consists of the real-time operating costs of DSO electrical, heating energy, and cooling energy distributed generation units ($P^{DG}_{i\ DS}(t) \cdot \gamma_{i\ DS}(t), H^{HDER}_{i\ DS}(t) \cdot \gamma'_{i'DS}(t), R^{CDER}_{i\ DS}(t) \cdot \gamma''_{i''DS}(t)$), the costs of IBEDRP paid to MGs ($C^{IBEDR\_RT}_{j\ MG}(t)$), the costs of IBHDRP paid to MGs ($C^{IBHDR\_RT}_{j'MG}(t)$), the costs of IBCDRP paid to MGs ($C^{IBCDR\_RT}_{j''MG}(t)$), the costs of PBEDRP paid to MGs ($C^{PBEDR\_RT}_{g\ MG}(t)$), the costs of PBHDRP paid to MGs ($C^{PBHDR\_RT}_{g'MG}(t)$), the costs of PBCDRP paid to MGs ($C^{PBCDR\_RT}_{g''MG}(t)$), costs of electricity, heating, and cooling energy purchased from electrical, heating and cooling energy market ($C^{IMPORT\_RT}_{DS}(t)$), and benefit of electrical energy ($B^{E\_EXPORT\_RT}_{DS}(t)$), heating energy ($B^{H\_EXPORT\_RT}_{DS}(t)$), and cooling energy ($B^{C\_EXPORT\_RT}_{DS}(t)$) sold to the electricity market, heating energy market, and cooling energy market, respectively.

The second term of Eq. (29) can be presented as (31):

$$\begin{aligned} \mathbb{A}^{RT}_{s\ DS}(t) = & \sum_{i=1}^{NIDG} C^{IDG}_{(i,s)\ DS}(t) + \sum_{g=1}^{G} VC^{PBEDR\_RT}_{(g,s)\ MG}(t) + \sum_{g'=1}^{G'} VC^{PBHDR\_RT}_{(g',s)\ MG}(t) + \sum_{g''=1}^{G''} VC^{PBCDR\_RT}_{(g'',s)\ MG}(t) + \\ & ECIC_{DS}(t) + HCIC_{DS}(t) + CCIC_{DS}(t) \end{aligned} \tag{31}$$

where the $\mathbb{G}^{RT}_{DS}(t)$ can be represented as (30):

$$\begin{aligned} \mathbb{G}^{RT}_{DS}(t) = & \sum_{i=1}^{NDG} \left[P^{DG}_{i\ DS}(t) \cdot \gamma_{i\ DS}(t) \right] + \sum_{i'=1}^{NHDER} \left[H^{HDER}_{i\ DS}(t) \cdot \gamma'_{i'DS}(t) \right] + \\ & \sum_{i''=1}^{NCDER} \left[R^{CDER}_{i\ DS}(t) \cdot \gamma''_{i''DS}(t) \right] + \sum_{j=1}^{J} C^{IBEDR\_RT}_{j\ MG}(t) + \sum_{j'=1}^{J'} C^{IBHDR\_RT}_{j'MG}(t) + \sum_{j''=1}^{J''} C^{IBCDR\_RT}_{j''MG}(t) + \\ & \sum_{g=1}^{G} C^{PBEDR\_RT}_{g\ MG}(t) + \sum_{g'=1}^{G'} C^{PBHDR\_RT}_{g'MG}(t) + \sum_{g''=1}^{G''} C^{PBCDR\_RT}_{g''MG}(t) + C^{IMPORT\_RT}_{DS}(t) \\ & - B^{E\_EXPORT\_RT}_{DS}(t) - B^{H\_EXPORT\_RT}_{DS}(t) - B^{C\_EXPORT\_RT}_{DS}(t) \end{aligned} \tag{30}$$

Table 2
The characteristics of distributed energy resources of microgrids.

CCHP	Electrical efficiency	0.45	Thermal efficiency	0.3
CCHP	Maximum electrical power output	20 kW	Maximum thermal power output	20 kW
Boiler	Efficiency	0.9	Maximum thermal power output	40 kW
Electrical chiller	Efficiency	0.85	Maximum thermal power output	30 kW
Absorption chiller	Efficiency	0.90	Maximum thermal power output	25 kW

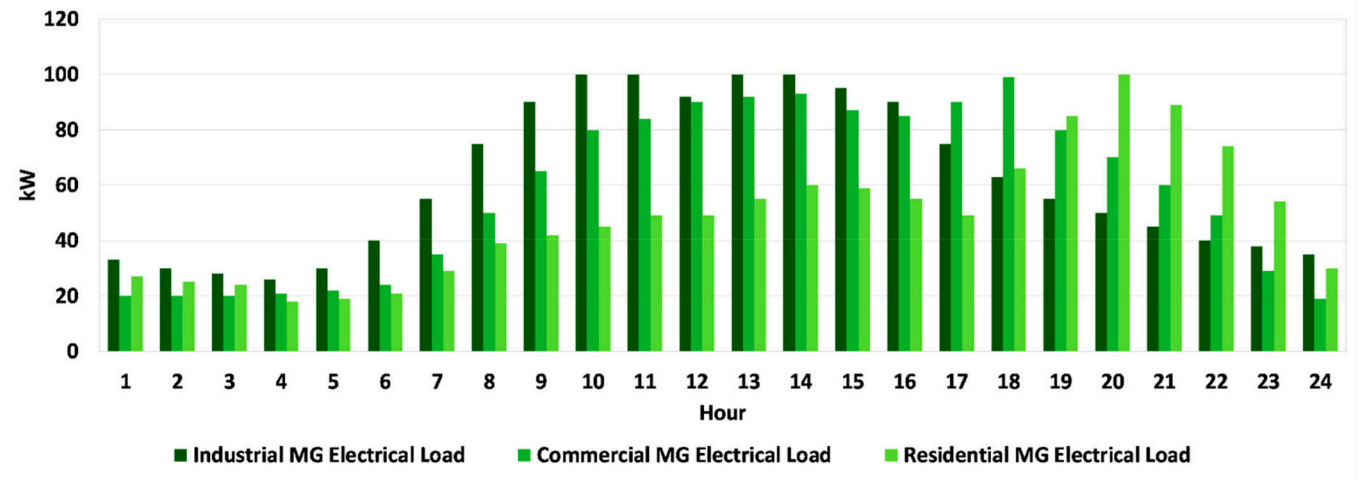

(a)

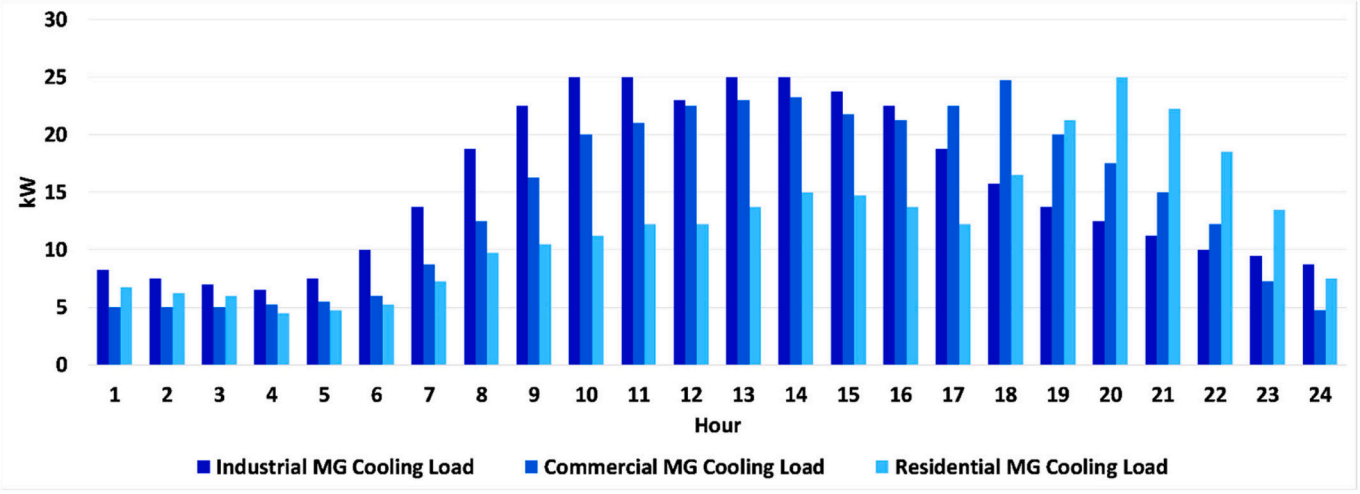

(b)

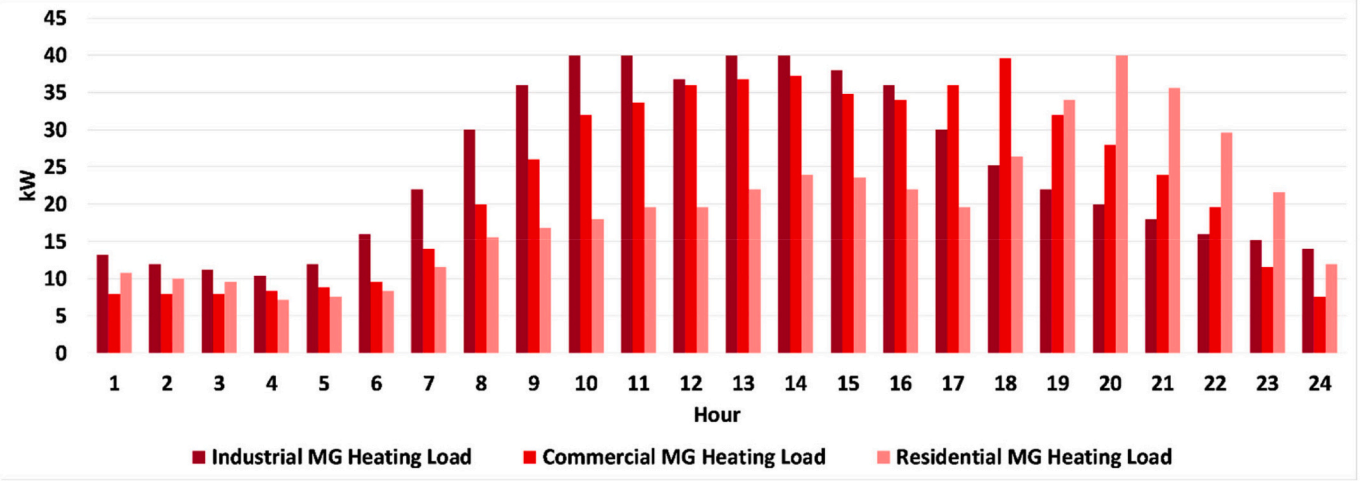

(c)

Fig. 9. (a) The electrical loads of MGs for one of the reduced scenarios., (b) The heating loads of MGs for one of the reduced scenarios., (c) The cooling loads of MGs for one of the reduced scenarios.

Eq. (31) consists of the operating costs of DSO's intermittent electricity facilities ($C^{IDG}_{(i,s)\ DS}(t)$), the variable costs of PBEDRP paid to MGs ($VC^{PBEDR\_RT}_{(j,s)\ MG}(t)$), the variable costs of PBHDRP paid to MGs ($VC^{PBHDR\_RT}_{(j',s)\ MG}(t)$), the variable costs of PBCDRP paid to MGs ($VC^{PBCDR\_RT}_{(j'',s)\ MG}(t)$), the electrical energy not supplied costs ($ECIC_{DS}(t)$), the heating energy not supplied costs ($HCIC_{DS}(t)$), the cooling energy not supplied costs ($CCIC_{DS}(t)$).

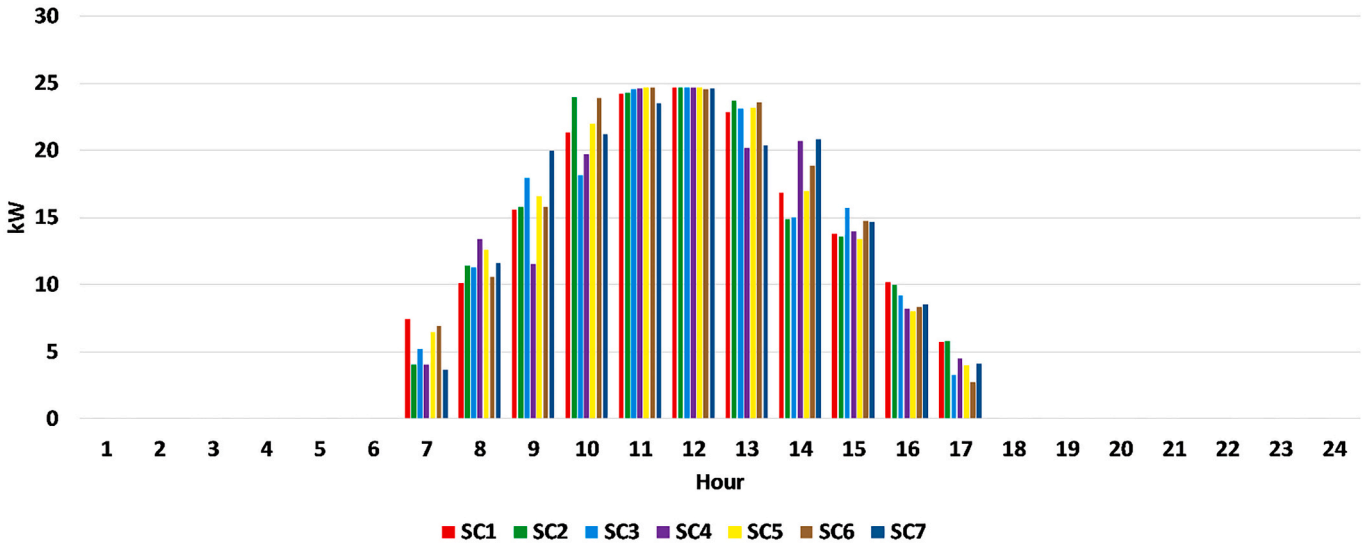

Fig. 10. The average values of the electrical power output of residential, commercial, and industrial MGs' wind turbines for different scenarios.

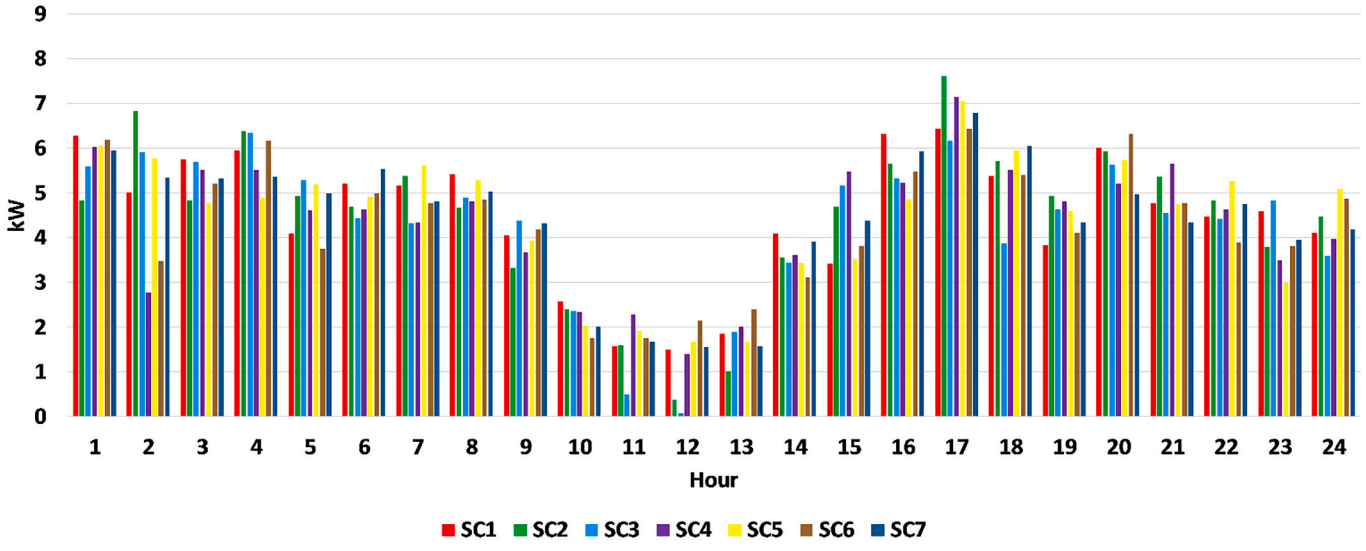

Fig. 11. The average values of the electrical power output of residential, commercial, and industrial MGs' photovoltaic systems for different scenarios.

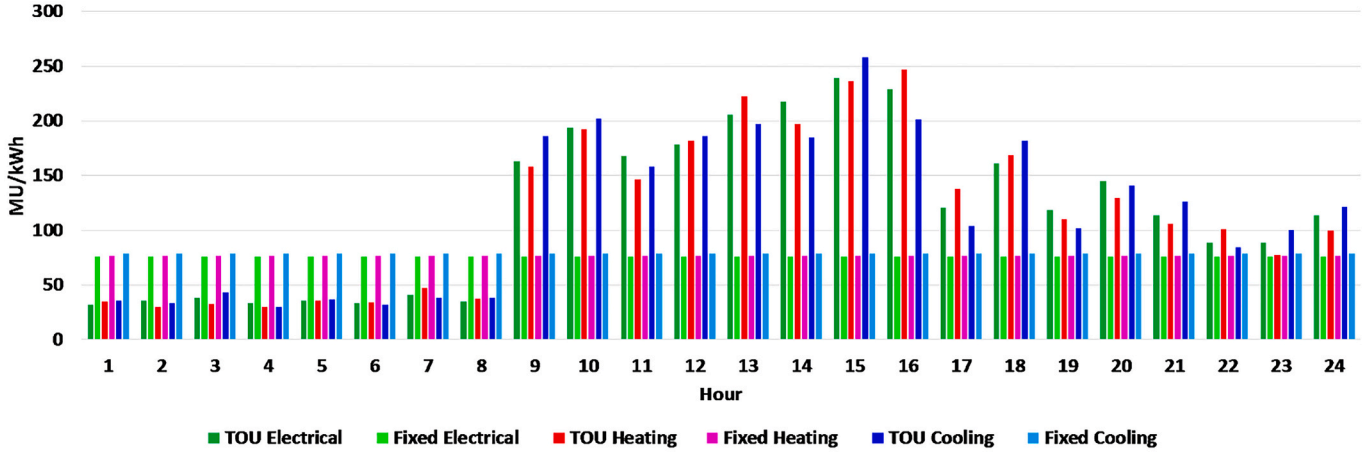

Fig. 12. The values of fixed and time-of-use prices of energy system for electrical, heating, and cooling loads.

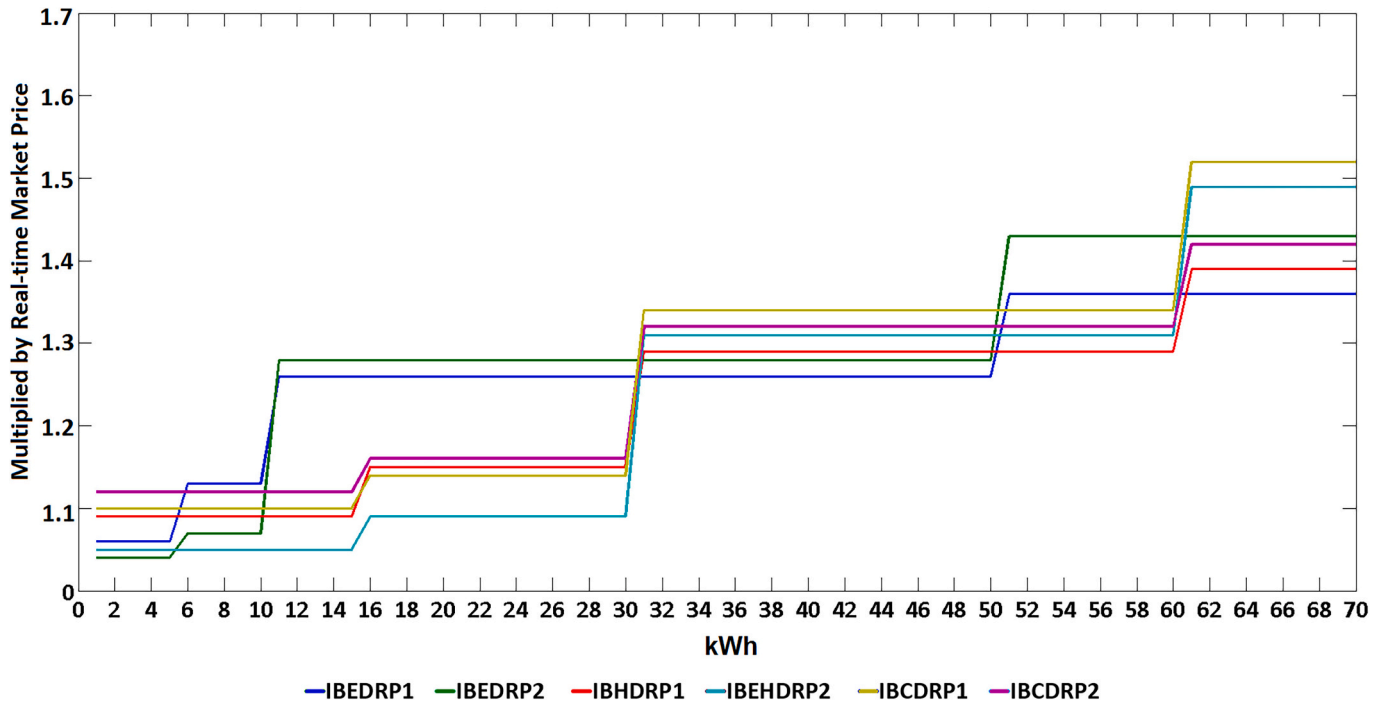

Fig. 13. The value of incentive-based electrical, heating, and cooling demand response programs for MGs.

Table 3
The feasible switching alternatives of electric switches and control valves of district heating and cooling networks.

Topology Number	Number of ES&CV							
1	1	0	1	0	0	1	0	0
2	1	1	1	0	1	1	0	0
3	1	0	1	0	0	1	0	0
4	0	0	1	0	0	1	0	0
5	0	1	1	0	0	1	0	0
6	1	0	1	0	0	1	1	1
7	1	0	1	0	0	1	1	0
8	1	0	1	0	0	1	0	0
9	1	0	1	0	0	1	0	0
10	1	0	1	1	1	0	1	0
11	0	0	1	0	0	1	0	0
12	1	0	1	1	0	1	0	0
13	1	0	1	1	0	1	0	0
14	1	1	1	0	0	1	0	0
15	1	0	1	0	0	1	0	1
16	1	0	1	0	0	1	1	1

The third term of Eq. (29) can be presented as (32):

$$\mathbb{B}_{DS}^{RT}(t) = TENP_{DG\ DS}(t) + TENP_{Market\ DS}(t) \tag{32}$$

Eq. (32) consists of the volume of environmental pollution of DSO's distributed generation units and the fossil-fueled electricity generation of wholesale market units, respectively.

The proposed objective function has the same constraints as the day-ahead problem.

A Multi-Carrier Energy System Resiliency Index (*MCESRI*) is utilized to assess the resiliency level of the energy system. The *MCESRI* is defined as (33):

$$MCESRI = \sum_{k=1}^{NCEL} P_{Critical} \Big/ \left(\sum_{k=1}^{NEL} P_0 - \sum_{k=1}^{NCEL} P_{Critical} \right) + \sum_{k'=1}^{NCHL} H_{Critical} \Big/ \left(\sum_{k'=1}^{NHL} H_0 - \sum_{k'=1}^{NCHL} H_{Critical} \right) + \sum_{k''=1}^{NCCL} R_{Critical} \Big/ \left(\sum_{k''=1}^{NCL} R_0 - \sum_{k''=1}^{NCCL} R_{Critical} \right) \tag{33}$$

where, $P_{Critical}, H_{Critical}, R_{Critical}$ are the critical values of electrical loads, heating loads, and cooling loads, respectively. Further, P_0, H_0, R_0 are the sum of critical and non-critical electrical loads, heating loads, and cooling loads, respectively.

2.8. The objective function of MGs for real-time operational scheduling problem (Second level of real-time optimization process)

As shown in Fig. 2, the MGs can transact energy carriers with the DSO. The MG operator should minimize operating costs and maximize the profits of energy transactions with the DSO. Further, the MG operator should minimize the penalty costs of any deviation between day-ahead accepted values and their real-time operating variables. Finally, the interruption costs of MG's loads should be minimized. The proposed real-time objective function is formulated as (34):

$$Min\ F_{MG}^{RT}(x) = \sum_{k=1}^{NRTST} \left[\mathfrak{W}_{MG}^{RT}(t) + \mathfrak{U}_{MG}^{RT}(t) + \mathbb{S}_{MG}^{RT}(t) \right] \tag{34}$$

where $\mathfrak{W}_{MG}^{RT}(t)$ can be presented as (35):

Table 4
The nine cases of demand response alternatives that the simulation processes were carried out.

Case	RTP (without IBDRP)	RTP (with IBDRP1)	RTP (with IBDRP2)	TOU (without IBDRP)	TOU (with IBDRP1)	TOU (with IBDRP2)	Fixed Price
1							
2							
3							
4							
5							
6							
7							
8							
9							
10							
11							
12							
13							
14							
15							
16							
17							
18							
19							
20							
21							

Minimization of operating costs

Minimizing of emission pollution

Minimization of operating costs and emissions pollution

$$\begin{aligned}\mathfrak{M}_{MG}^{RT}(t) = \; & \sum_{i=1}^{NDG'}\left[P_{i\,MG}^{DG}(t)\cdot\gamma_{i\,MG}(t)\right] + \sum_{i=1}^{NHRMG}\left[H_{i\,MG}^{HDER}(t)\cdot\gamma'_{iMG}(t)\right]+ \\ & \sum_{i''=1}^{NCRMG}\left[R_{i\,\mathrm{MG}}^{CDER}(t)\cdot\gamma''_{i\mathrm{MG}}(t)\right] + \sum_{j=1}^{J} B_{j\,MG}^{IBEDR\_RT}(t) + \sum_{j'=1}^{J'} B_{j'MG}^{IBHDR\_RT}(t)+ \\ & \sum_{j''=1}^{J''} B_{j''MG}^{IBCDR\_RT}(t) + \sum_{g=1}^{G} B_{g\,MG}^{PBEDR\_RT}(t) + \sum_{g'=1}^{G'} B_{g'MG}^{PBHDR\_RT}(t) + \sum_{g''=1}^{G''} B_{g''MG}^{PBCDR\_RT}(t)+ \\ & C_{MG}^{IMPORT\_RT}(t) - B_{MG}^{EXPORT\_RT}(t)\end{aligned} \tag{35}$$

Eq. (35) consists of the operating costs of distributed generation units ($P_{i\,MG}^{DG}(t)\cdot\gamma_{i\,MG}(t)$, $H_{i\,MG}^{HDER}(t)\cdot\gamma'_{iMG}(t)$, $R_{i\,MG}^{CDER}(t)\cdot\gamma''_{iMG}(t)$), the benefits of IBEDRP ($C_{j\,MG}^{IBEDR\_RT}(t)$), the benefits of IBHDRP ($C_{j'MG}^{IBHDR\_RT}(t)$), the benefits of IBCDRP ($C_{j''MG}^{IBCDR\_RT}(t)$), the benefits of PBEDRP ($C_{g\,MG}^{PBEDR\_RT}(t)$), the benefits of PBHDRP ($C_{g'MG}^{PBHDR\_RT}(t)$), the benefits of PBCDRP ($C_{g''MG}^{PBCDR\_RT}(t)$), costs of electricity, heating and cooling energy purchased from DSO ($C_{MG}^{IMPORT\_RT}$), and benefit of electrical, heating, and cooling energy sold to DSO ($B_{MG}^{EXPORT\_RT}$).

The $\mathfrak{N}_{s\,MG}^{RT}(t)$ term is formulated as (36):

$$\begin{aligned}\mathfrak{N}_{s\,MG}^{RT}(t) = & \sum_{i=1}^{NIDG'} C_{(i,s)\;MG}^{IDG}(t) + \sum_{j=1}^{J} Penalty_{(g,s)\;MG}^{IBEDR\_RT}(t)+ \\ & \sum_{j'=1}^{J'} Penalty_{(g',s)\;MG}^{IBHDR\_RT}(t) + \sum_{j''=1}^{J''} Penalty_{(g'',s)\;MG}^{IBCDR\_RT}(t)+ \\ & ECIC_{MG}(t) + HCIC_{MG}(t) + CCIC_{MG}(t)\end{aligned} \tag{36}$$

Eq. (36) consists of the operating costs of MG's intermittent electricity facilities ($C_{(i,s)\;MG}^{IDG}(t)$), the penalty costs of MG's IBEDRP ($Penalty_{(j,s)\;MG}^{IBEDR\_RT}(t)$), the penalty costs of MG's IBHDRP

Table 5
The average costs of residential, industrial, and commercial microgrids for the twenty-one case studies.

			RTP (without IBDRP)	RTP (with IBDRP1)	RTP (with IBDRP2)	TOU (without IBDRP)	TOU (with IBDRP1)	TOU (with IBDRP2)	Fixed Price
Industrial Microgrid	Minimization of operating costs	Operating costs (MUs)	57121	55219	54902	60660	59064	58847	68447
		Emission pollution (kg)	146920	143184	142992	144406	141209	141209	161919
	Minimizing of emission pollution	Operating costs (MUs)	146041	146115	148839	146041	146115	148839	146041
		Emission pollution (kg)	110657	108696	108696	110657	108696	108696	110657
	Minimization of operating costs and emission pollution	Operating costs (MUs)	57121	55219	54902	60660	59064	58847	68447
		Emission pollution (kg)	146920	143184	142992	144406	143209	144209	161919
Commercial Microgrid	Minimization of operating costs	Operating costs (MUs)	146041	146115	148839	146041	146115	148839	146041
		Emission pollution (kg)	110657	108696	108696	110657	108696	108696	110657
	Minimizing of emission pollution	Operating costs (MUs)	69855	66945	66772	71966	69764	69821	100454
		Emission pollution (kg)	126267	125661	125192	125501	124661	124212	116834
	Minimization of operating costs and emission pollution	Operating costs (MUs)	69117	66293	65333	68546	72057	73559	76661
		Emission pollution (kg)	174834	161821	158721	167511	168039	163802	202399
Residential Microgrid	Minimization of operating costs	Operating costs (MUs)	169407	160726	181583	163566	182644	174141	181090
		Emission pollution (kg)	125042	122826	128261	128362	119565	127174	138321
	Minimizing of emission pollution	Operating costs (MUs)	82429	79665	78123	87079	86508	83086	122554
		Emission pollution (kg)	147733	157076	138963	148091	145853	150296	136696
	Minimization of operating costs and emission pollution	Operating costs (MUs)	63976	62949	60941	69153	64970	66497	76671
		Emission pollution (kg)	166019	163366	160151	169291	168154	166742	182969

($Penalty^{IBHDR\_RT}_{(j',s)\ MG}(t)$), the penalty costs of MG's IBCDRP ($Penalty^{IBCDR\_RT}_{(j',s)\ MG}(t)$), the MG's electrical consumer interruption costs ($ECIC_{MG}(t)$), the MG's heating consumer interruption costs ($HCIC_{MG}(t)$), the MG's heating consumer interruption costs ($CCIC_{MG}(t)$).

The $\mathbb{S}^{RT}_{MG}(t)$ term is the same as $\mathbb{S}^{DA}_{MG}(t)$. The constraints of the real-time proposed objective function are the same as the day-ahead objective function constraints and are not presented for the sake of space.

3. Solution algorithm

As shown in Fig. 3, the proposed model is an iterative two-stage two-level optimization process. The following assumptions are considered in the method:

- The Auto-Regressive Integrated Moving Average (ARIMA) models were utilized to generate scenarios for the following stochastic processes: hourly electrical, heating, and cooling demand profiles, day-ahead prices of electricity, heating, and cooling markets, hourly charge and discharge of PHEVs' parking lots, MGs' energy transactions and energy consumptions, wind turbine, and photovoltaic electricity generation, and real-time prices of electricity, heating, and cooling markets. The detailed formulations of ARIMA models for generating scenarios for stochastic processes are available in [26].
- However, solving the optimization problem for the generated scenarios was very time-consuming. Thus, a scenario reduction process was utilized. The forward selection method was used to reduce the generated scenarios [27]. The total number of scenarios was 10,007,

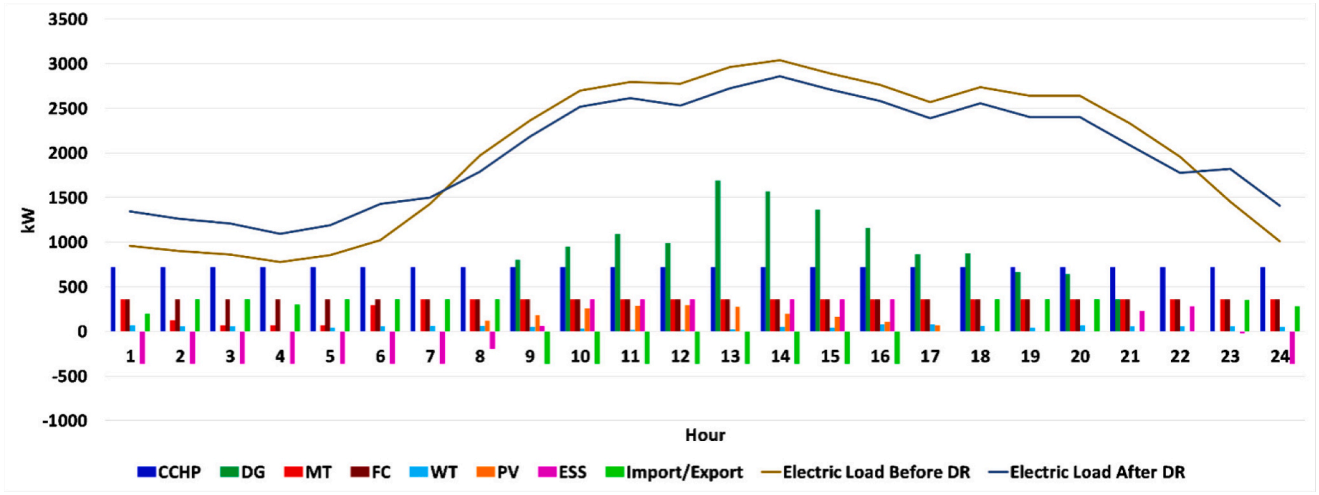

(a)

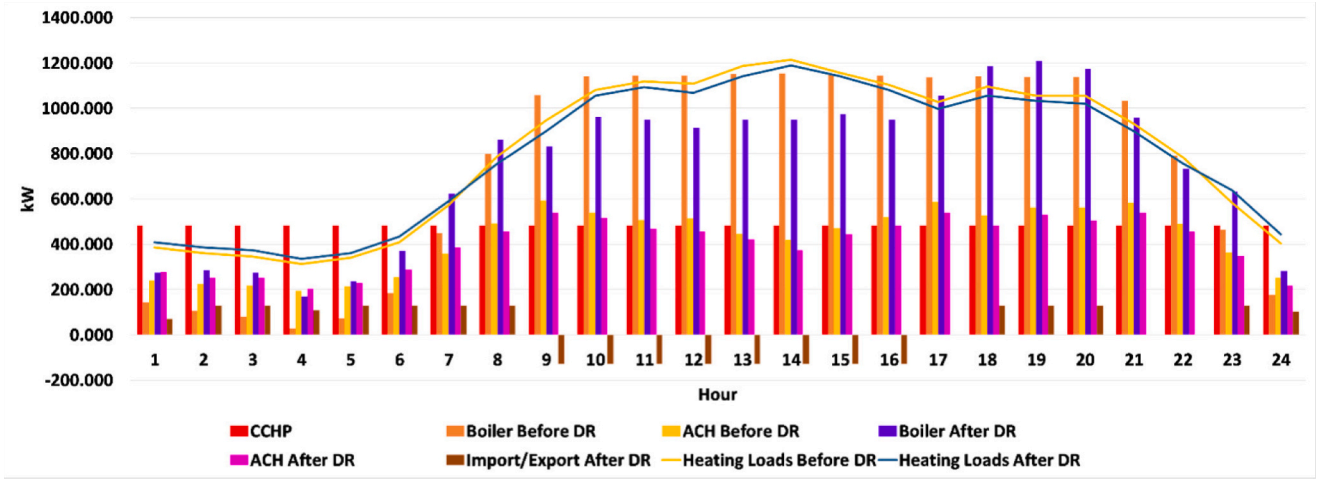

(b)

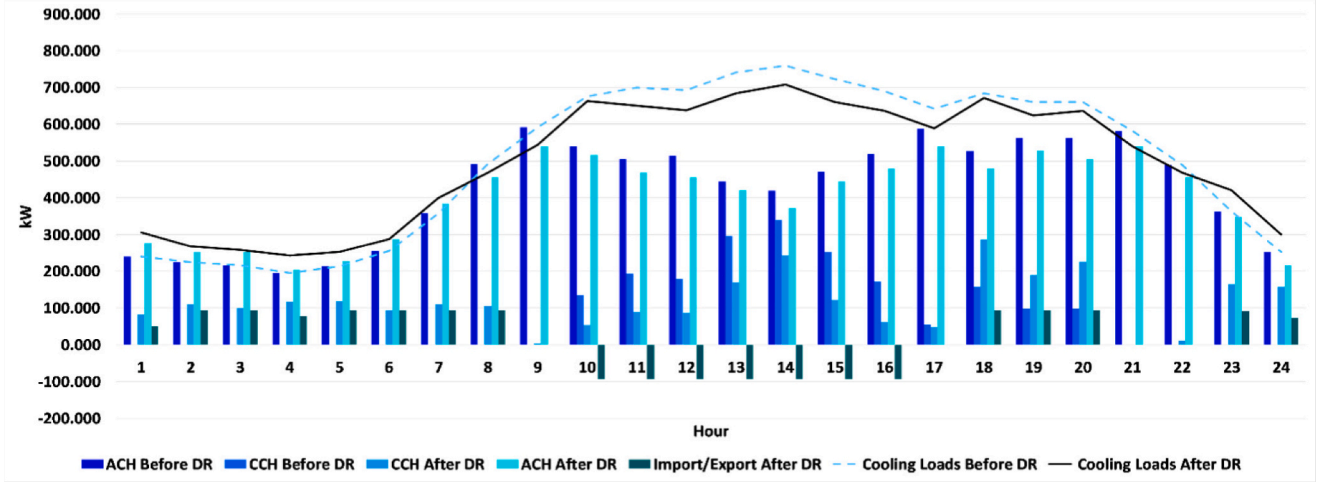

(c)

Fig. 14. (a). The aggregated values of optimal day-ahead electrical, distributed energy resources of MGs for IBDRP1 case, (b) the aggregated values of optimal day-ahead heating distributed energy resources of MGs for IBDRP1 case, (c) the aggregated values of optimal day-ahead cooling distributed energy resources of MGs for IBDRP1 case.

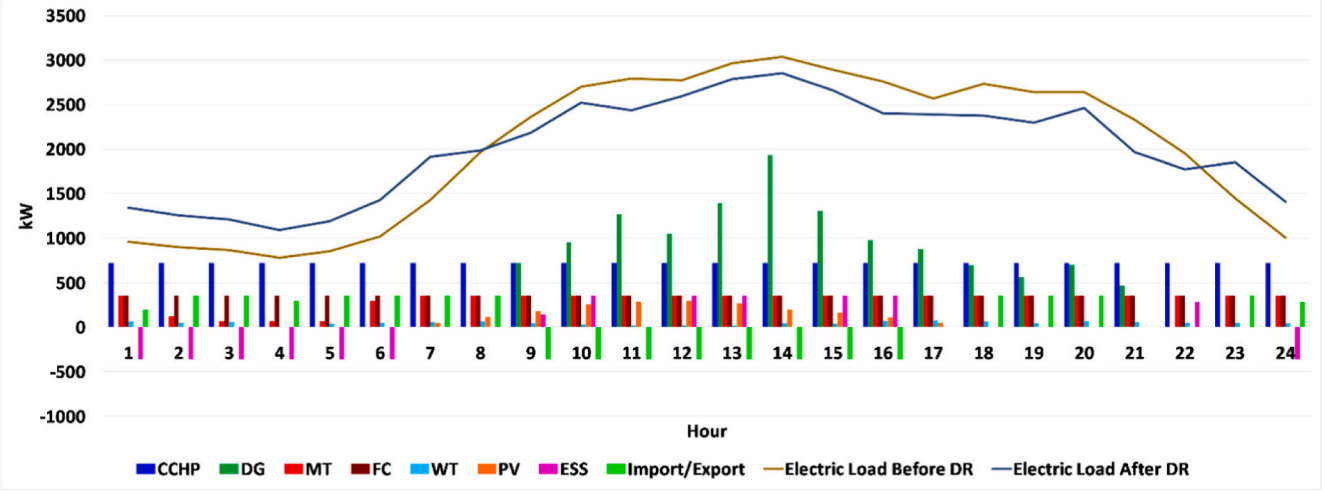

(a)

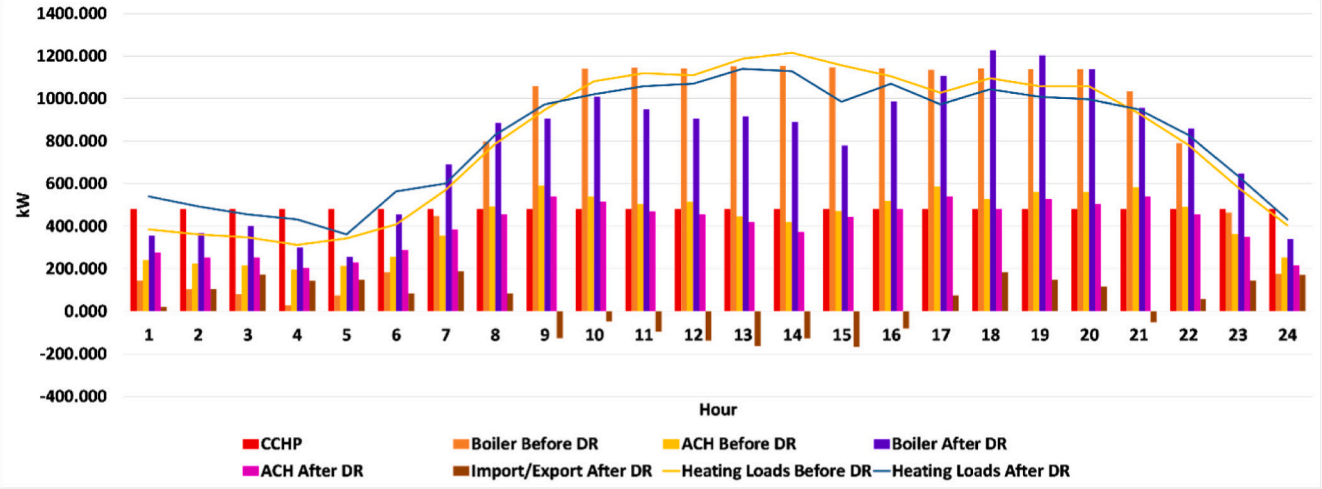

(b)

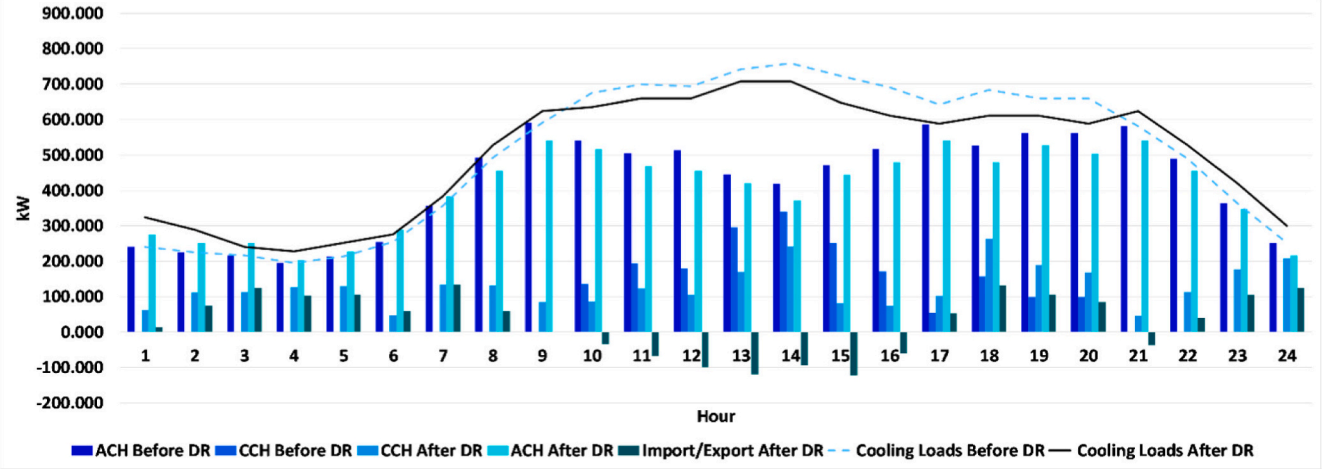

(c)

Fig. 15. (a). The aggregated values of optimal day-ahead electrical, distributed energy resources of MGs for IBDRP2 case, (b) the aggregated values of optimal day-ahead heating distributed energy resources of MGs for IBDRP2 case, (c) the aggregated values of optimal day-ahead cooling distributed energy resources of MGs for IBDRP2 case.

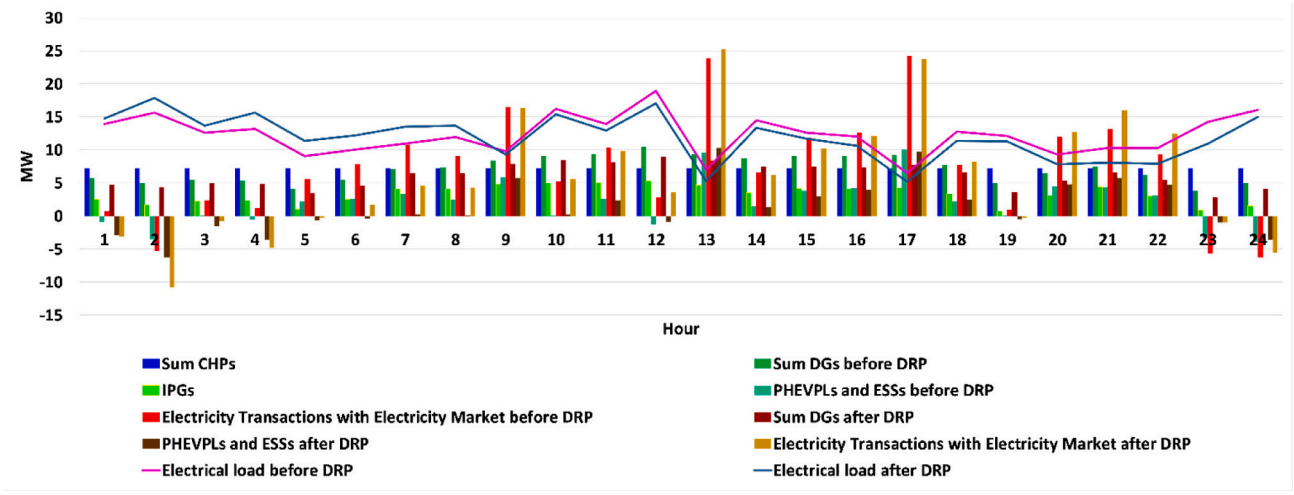

(a)

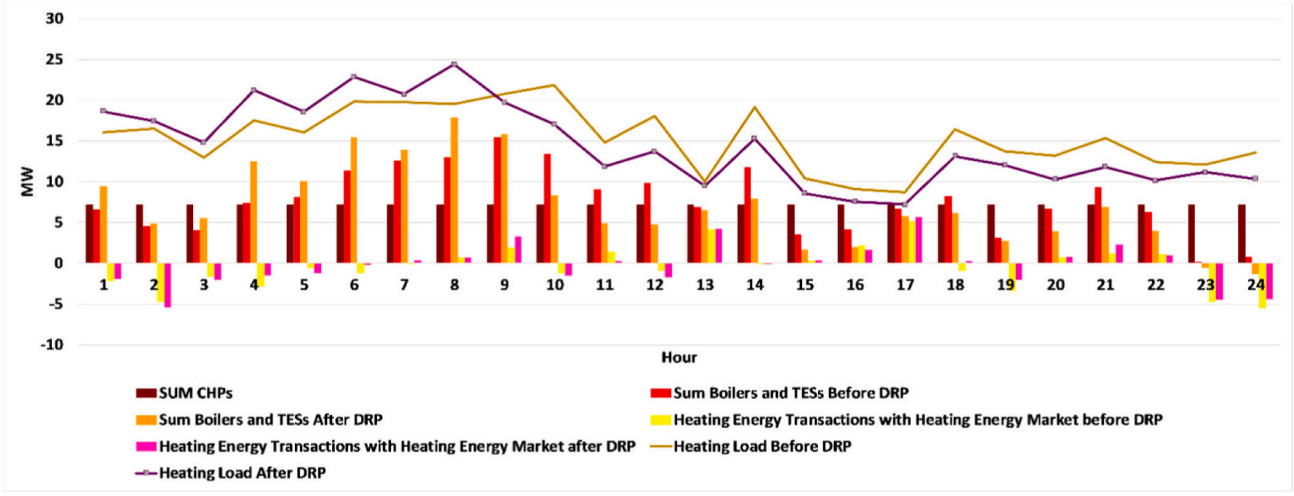

(b)

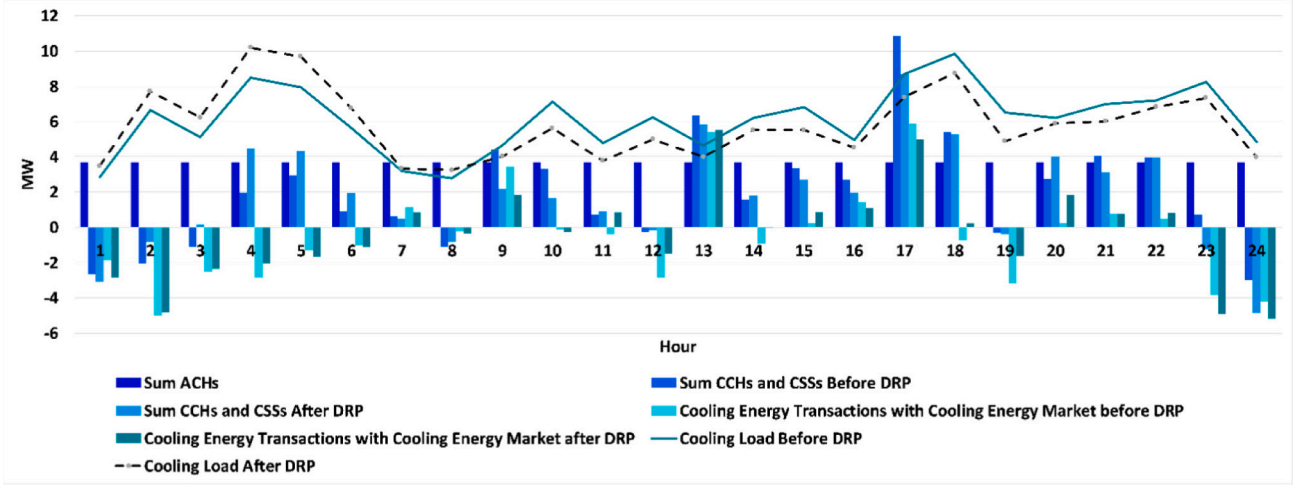

(c)

Fig. 16. (a). The aggregated values of optimal day-ahead electrical, distributed energy resources of the energy system for IBDRP2 case, (b) the aggregated values of optimal day-ahead heating distributed energy resources of the energy system for IBDRP2 case, (c) the aggregated values of optimal day-ahead cooling distributed energy resources of the energy system for IBDRP2 case.

which led to the curse of dimensionality. The scenario reduction method reduced the scenarios to 10 each.

- The Monte Carlo simulation process was utilized to estimate the location and intensity of the external shocks [28]. For the Monte Carlo simulation, 300 trials were carried out to simulate the location and intensity of external shocks. For each external shock, the following contingencies were considered as the worst-case external shocks: 1) Triple energy carrier distribution network/pipeline outages and single DER outage; 2) Triple DER outages; and 3) Combination of described outages. It was assumed that each external shock shut down the described facilities for the entire time of the simulation process and the corrective switching process and dispatching of DERs were performed.
- For each external shock condition, the remaining energy system performance was optimized using the first level of the first stage optimization process. It was assumed that the external shock sectionalized the energy system into on-outage and secured zones [24]. Based on the proposed method, the energy system operator should

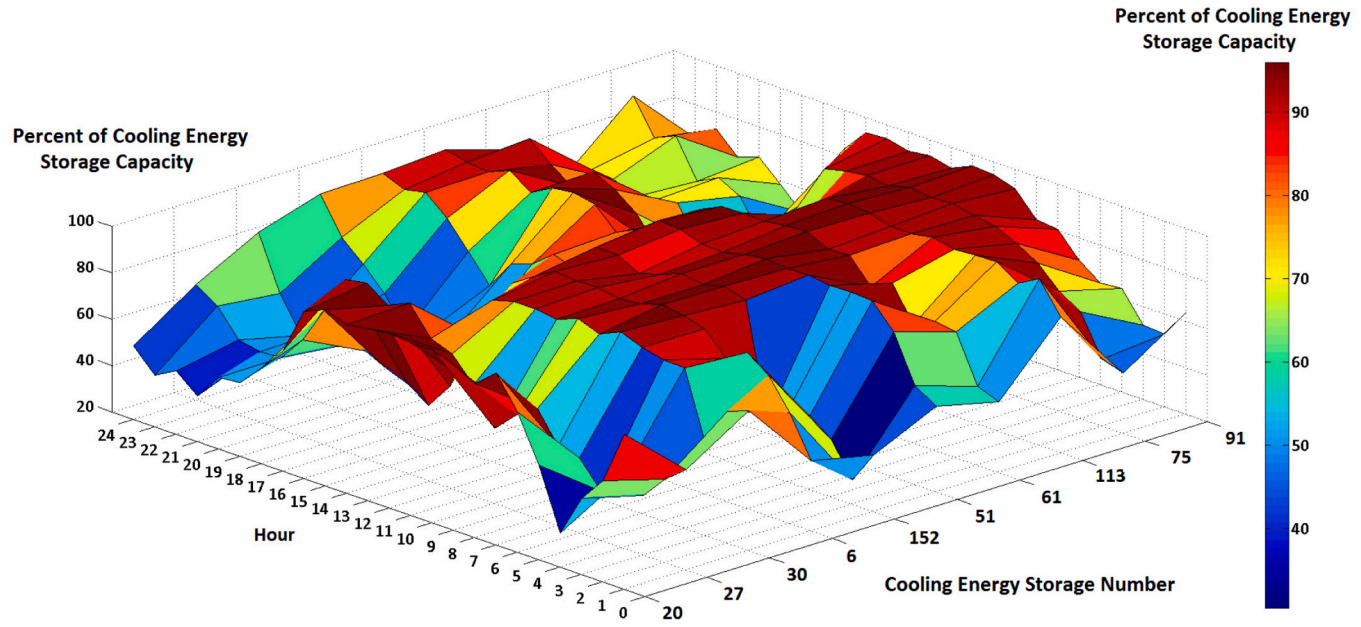

(a)

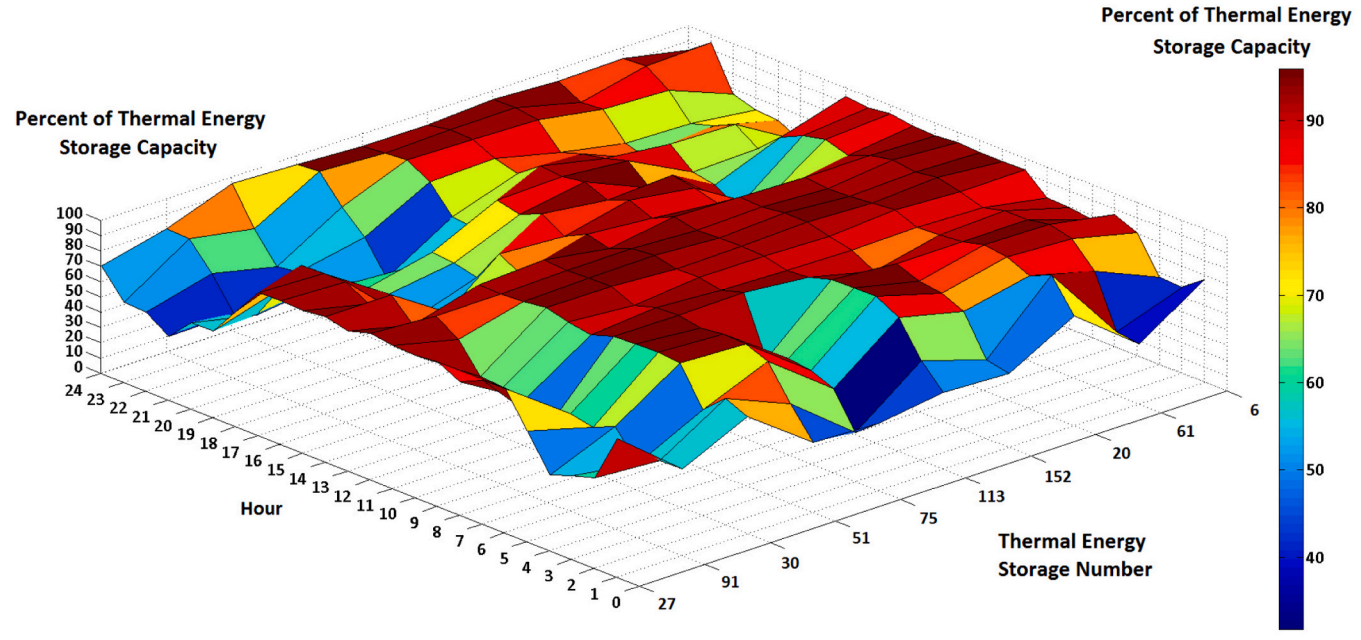

(b)

Fig. 17. (a). The optimal day-ahead dispatch of cooling energy storage of energy system for IBDRP2 case, (b) The optimal day-ahead dispatch of heating energy storage of energy system for IBDRP2 case, (c) The optimal day-ahead dispatch of cooling PHEV parking lots of energy system for IBDRP2 case.

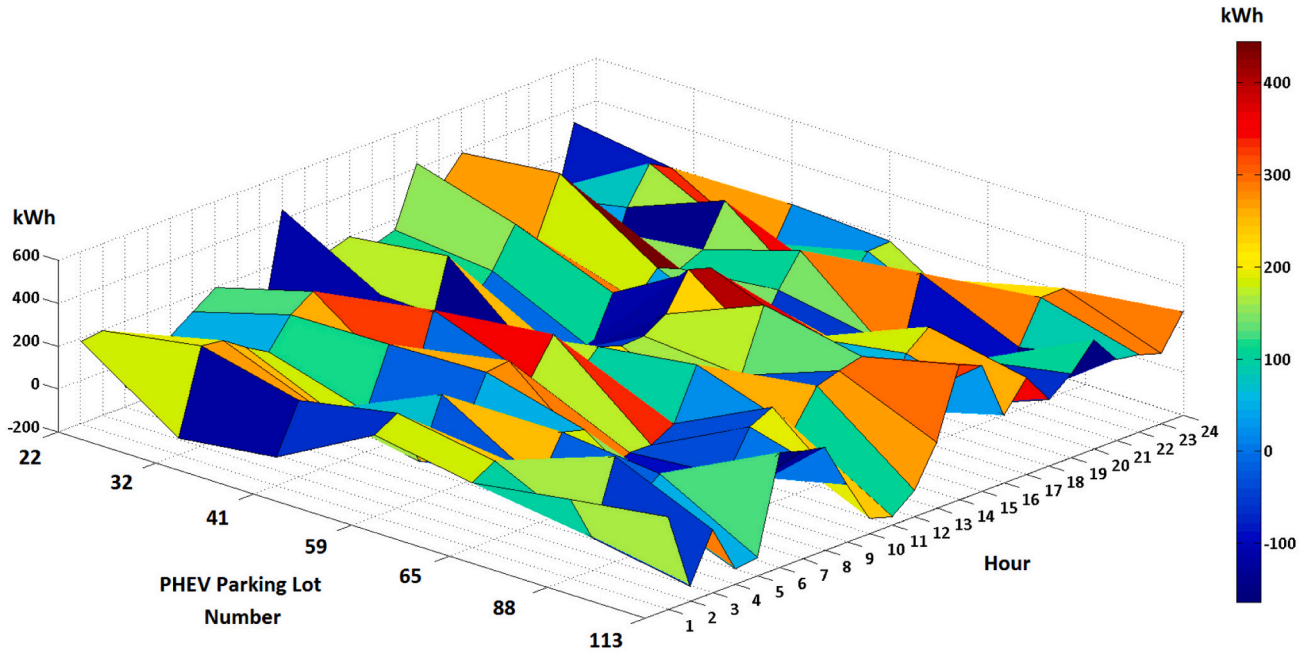

(c)

Fig. 17. (*continued*).

change the topology of electrical, heating, and cooling systems to restore the service for the on-outage zones using the DERs of neighbour-secured zones [24]. The detailed process of switching electrical switches, heating, and cooling valves is presented in [24] and is not presented for the sake of space.

- The second level of the second-stage optimization process determined the optimal contribution of MGs in external shock conditions. The MGs' DERs were dispatched for restoring the energy system using the switching process of electrical switches, and heating and cooling control valves.
- The simulation was carried out on a PC (Intel Core i7–13,700 processor, 128 GB memory, DDR4 3200 MT). The Monte Carlo simulation time was about 3485 seconds. The detailed process of the Monte-Carlo simulation process is available in [29] and is not presented for the sack of space.

The weighting factors are equal to one and the weighted sum method is carried out for the proposed objective functions.

The objective functions and their constraints problems are linearized [24].

The method codes are developed in MATLAB and GAMS.

Fig. 3 presents the flowchart of the method. As shown in Fig. 3, at the first level of the first stage optimization process, the energy system operator optimizes the day-ahead scheduling of the system's distributed energy resources and estimates the values of MGs' incentive-based and price-based demand response contributions. Then, the second level of the first stage optimization process determines the optimal scheduling of MGs' DERs and incentive-based and price-based demand response variables. It is assumed that based on the outputs of the second level of the first stage optimization problem, which update the data of MG's DERs decision variables and incentive-based and price-based demand response variables, the first level of the first stage objective function can be recalculated and the day-ahead optimal scheduling of energy system can be determined.

In the real-time scheduling process, if there is not any shock, the process simulates the shock conditions and the first and second levels of second-stage optimization processes determine the optimal dispatch of distributed energy resources of energy systems and MGs, respectively. The simulation of an external shock is performed to assess the behavior of the energy system in contingent conditions and find the optimal preventive scheduling of energy resources and available alternatives for system reconfiguration. This process should be carried out to reduce the impacts of external shock. Further, the available dispatching strategies of the energy system operator against probable shocks can be explored using the simulation process of external shock conditions.

Based on the proposed method, in real-time operating conditions, if any shock condition is detected, the real-time optimization processes determine the optimal commitment of the energy system's DERs, the system's topology, and MGs' optimal distributed energy generation commitments, which is one of the contributions of this paper. The optimization process minimizes the impacts of external shocks using the switching process of electrical switches and heating and cooling control valves.

4. Simulation results

The simulation was carried out for the modified 123-bus IEEE system. Fig. 4 depicts the system topology.

Fig. 5 depicts the electrical, heating, and cooling loads of the energy system. As shown in Fig. 5, the aggregated energy of electrical, heating, and cooling loads are 209.8 MWh, 367.77 MWH, and 146.38 MWH, respectively. Fig. 6 presents the energy generation of wind turbines and photovoltaic systems for one of the reduced scenarios. The estimated values of energy generation of wind turbines and photovoltaic arrays are 30.88 MWh and 47.685 MWh, respectively. Fig. 7 and Fig. 8 show the forecasted price of day-ahead and real-time multi-carrier energy markets, respectively. The details of system data are presented in [24] and are not presented for the sake of space.

The electrical, heating, and cooling demand of the microgrid was supplied by the microgrid multi-carrier distributed energy resources,

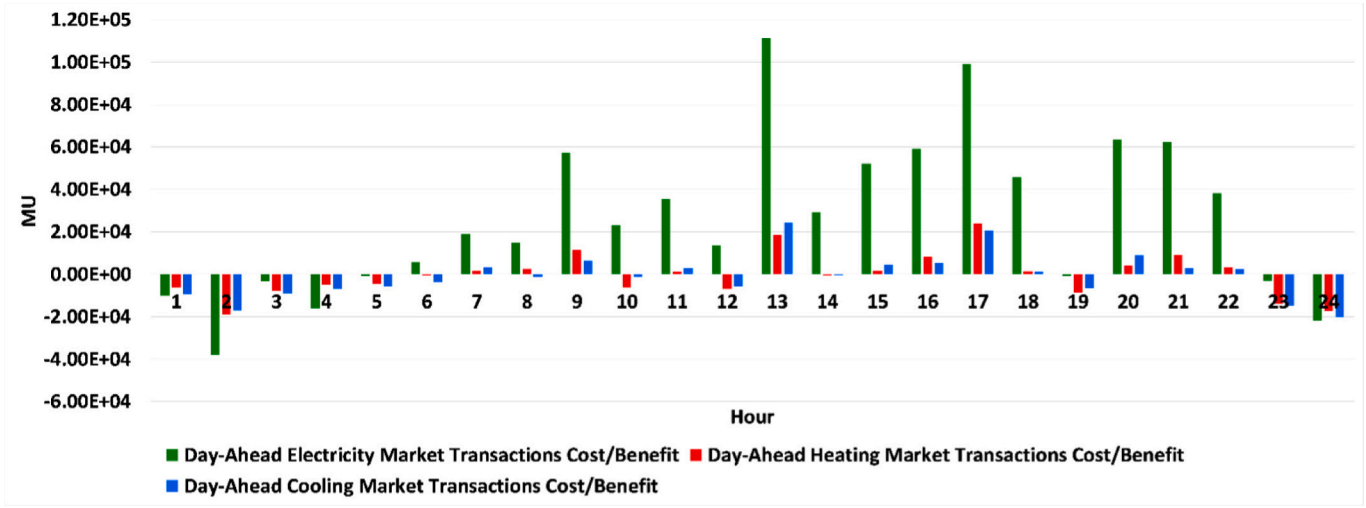

(a)

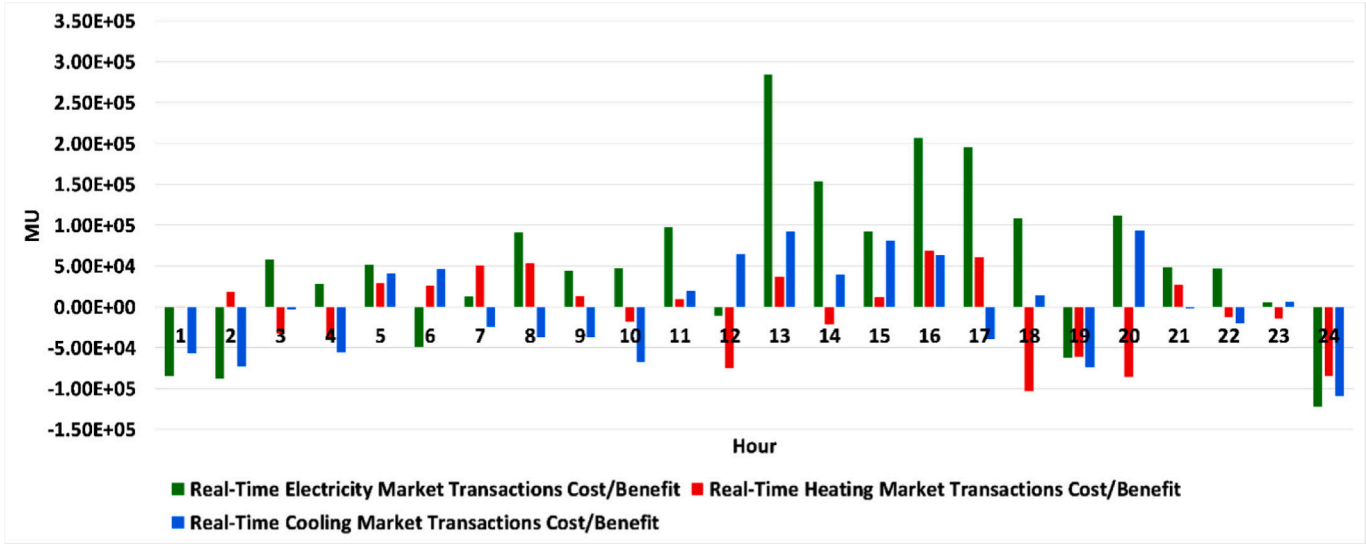

(b)

Fig. 18. (a). The day-ahead cost/benefit of energy system transactions with the multicarrier energy markets, and (b) the real-time cost/benefit of energy system transactions with the multicarrier energy markets.

which transacts electricity, heating, and cooling energy with multi-carrier energy markets. The microgrids are categorized into residential, commercial, and industrial microgrids. The characteristics of distributed energy resources of microgrids are presented in Table 2. The MGs data are available in [25] and are not presented for the sake of space. Further, the Eq. (16), Eq. (17), and Eq. (25) data are available in Ref. [25]. The interruption costs of electricity, heating, and cooling loads are considered 0.42 MMUs/kWh [24]. MMUs stands for Million Monetary Units.

Fig. 9. (a), (b), and (c) present the electrical, heating, and cooling loads of MGs for one of the reduced scenarios, respectively.

Fig. 10 depicts the average values of the electrical power output of residential, commercial, and industrial MGs' photovoltaic systems for different scenarios. As shown in Fig. 10, the average values of the electrical power output of residential, commercial, and industrial MGs' photovoltaic systems are 7.195 kWh, 7.169 kWh, 7.00 kWh, 6.901 kWh, 7.190 kWh, 7.277 kWh, and 7.216 kWh, respectively. Further, the aggregated values of the electrical power output of residential, commercial, and industrial MGs' photovoltaic systems are 172.700 kWh, 172.121 kWh, 165.636 kWh, 172.573 kWh, 174.670 kWh, and 173.188 kWh, respectively.

Fig. 11 shows the average values of the electrical power output of residential, commercial, and industrial MGs' wind turbines for different scenarios. As shown in Fig. 11, the average values of the electrical power output of residential, commercial, and industrial MGs' wind turbines are 4.499 kWh, 4.501 kWh, 4.310 kWh, 4.367 kWh, 4.461 kWh 7, 4.325 kWh, and 4.467 kWh, respectively. Further, the aggregated values of the electrical power output of residential, commercial, and industrial MGs' photovoltaic systems are 107.978 kWh, 108.041 kWh, 103.450 kWh, 104.828 kWh, 107.071 kWh, 103.820 kWh, and 107.213 kWh, respectively.

As presented in the problem formulations, different demand response programs are considered. Fig. 12 presents the value of fixed and time-of-use prices of the energy system for electrical, heating, and cooling loads.

As shown in Fig. 12, it is assumed that the reward of electrical, heating, and cooling loads in the time-of-use prices of price-based demand response process are equal to 120% of the average hourly prices of

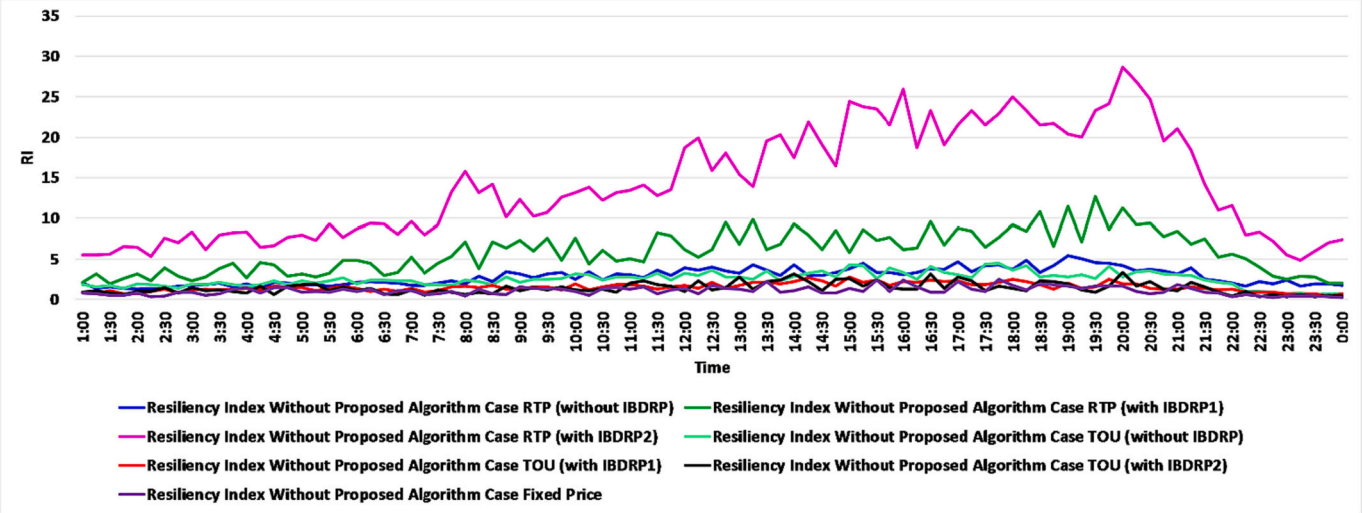

Fig. 19. The resiliency index of the energy system for the worst-case shock conditions considering different demand response programs and without the proposed method.

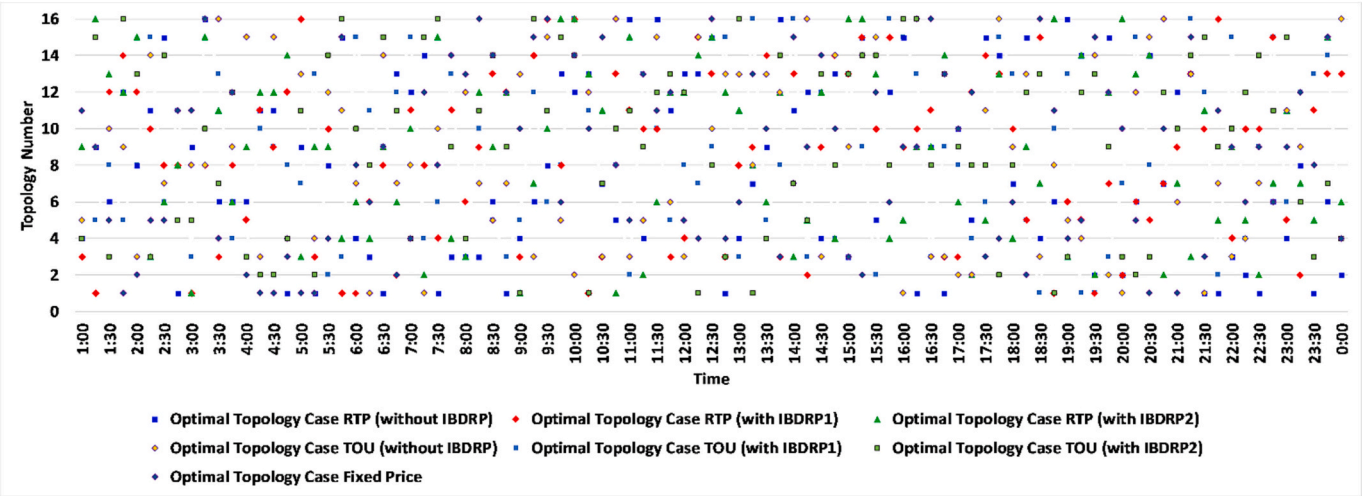

Fig. 20. The optimal topology number of the energy system for different demand response alternatives and the corresponding worst-case shock.

electrical, heating, and cooling markets, respectively. Further, the reward of electrical, heating, and cooling loads in the real-time prices of the price-based demand response process are equal to 110% of the real-time price of electrical, heating, and cooling markets, respectively.

Fig. 13 depicts the value of incentive-based electrical, heating, and cooling demand response programs for MGs that participate in multi-carrier energy markets based on their multi-carrier energy injections into energy system networks. As shown in Fig. 13, based on the volume of the energy injection of MGs into system energy, the incentive-based demand prices are multiplied by the corresponding real-time market.

It is assumed that the penalty costs of MGs for any deviation of incentive-based demand response programs in electrical, heating, and cooling markets are equal to 150% of their real-time market prices.

Table 3 depicts the feasible switching alternatives of Electric Switches and Control Valves (ES&CV) of district heating and cooling networks. As shown in Table 3, there are sixteen feasible topologies for the 123-bus system that the electrical, heating, and cooling loads can be supplied. The number of the external shock was forty cases and their impacts on the energy system were simulated. The worst-case scenario was considered as the following process. The first shock took place in energy corridor 160 at 15:00. The second shock came about in energy corridor 135 at 19:00.

Twenty-one simulation cases were carried out to assess the impacts of different demand response alternatives on the optimal scheduling of the energy system and microgrids, which Table. 4 depicts these cases.

Table 5 presents the average costs of residential, industrial, and commercial microgrids for the twenty-one case studies. As shown in Table 5, the real-time demand response integrated with the second package of incentive-based electrical, heating, and cooling demand response programs presented the minimum costs for microgrids considering simultaneous minimization of operating costs and emission pollution. The optimal incentive-based demand response program reduced the costs of residential microgrids by about 4.47% and 3.19% concerning the RTP and RTP (IBDRP1) cases, respectively. Further, the costs of industrial microgrids were reduced by about 3.88% and 0.57% concerning the RTP and RTP (IBDRP1) cases, respectively. Finally, the costs of commercial microgrids were reduced by about 5.47% and 1.44% concerning the RTP and RTP (IBDRP1) cases, respectively. Based on the Table. 5 results, the IBDRP2 and IBDRP1 alternatives were considered the first-best and second-best demand response program alternatives, respectively.

Based on the Table. 5 results, the IBDRP2 and IBDRP1 were

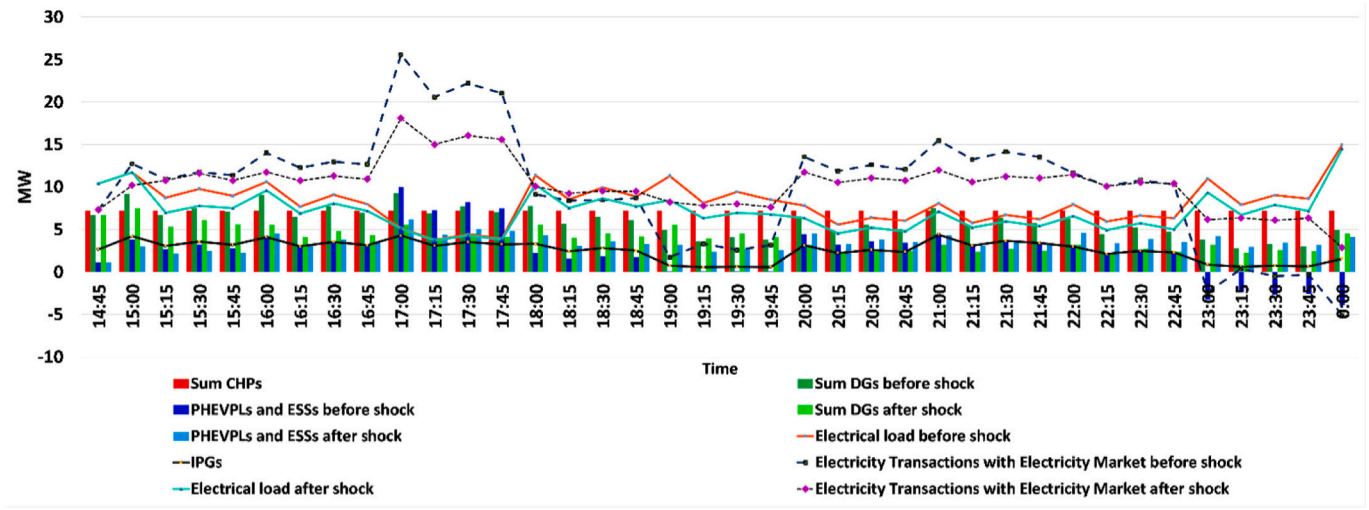

(a)

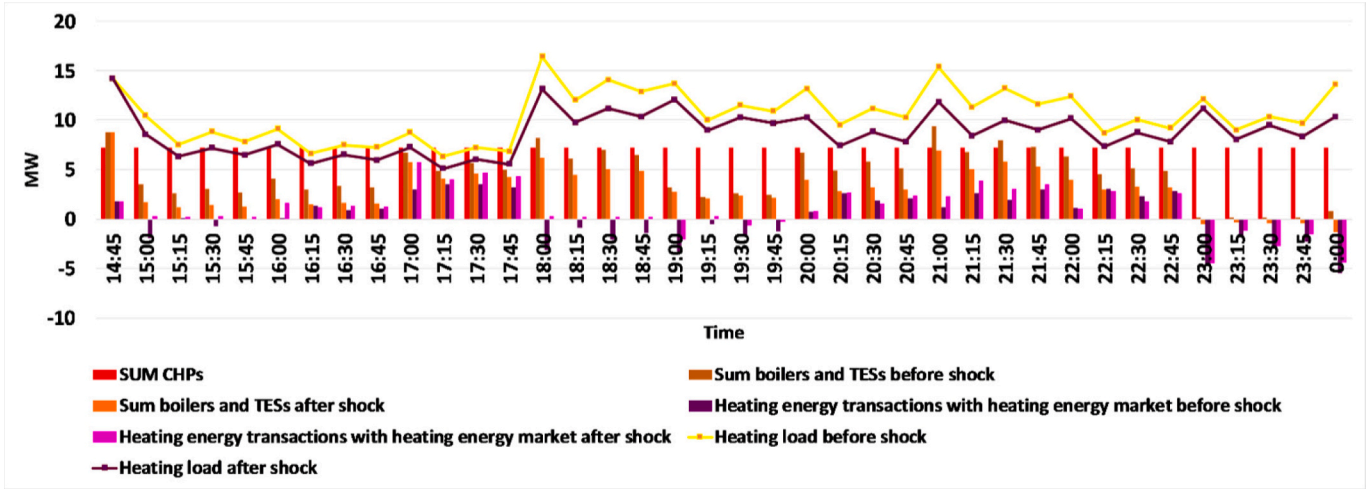

(b)

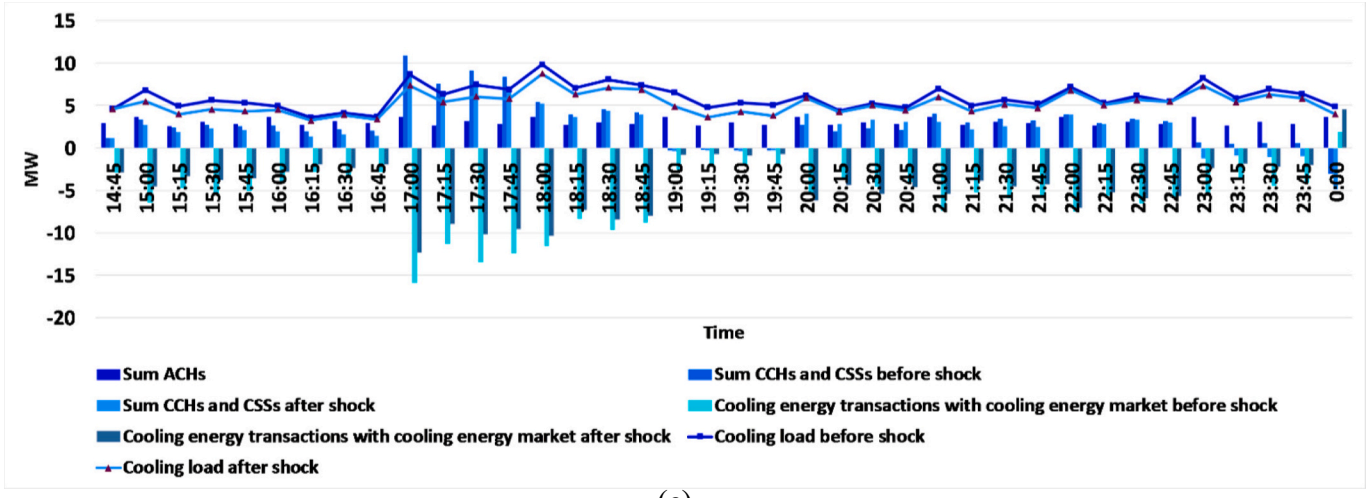

(c)

Fig. 21. (a). The optimal real-time dispatch of the electrical energy system for IBDRP2 case and worst-case shock, (b) The optimal real-time dispatch of the heating energy system for IBDRP2 case and worst-case shock, (c) The optimal real-time dispatch of the cooling energy system for IBDRP2 case and worst-case shock.

considered the first-best and second-best demand response alternatives, respectively. Thus, the MGs' commitments to these cases are presented.

Fig. 14 (a), (b), and (c) present the aggregated values of optimal day-ahead electrical, heating, and cooling distributed energy resources of MGs for the IBDRP1 case, respectively. Based on Fig. 14 (a), the aggregated electricity transactions of MGs with the energy system was 1494 kWh. Further, the aggregated electricity consumptions of MGs without and with IBDRP1 were 48,384 kWh and 48,384 kWh, respectively. Thus, the IBDRP1 process only changed the electrical load profile and did not reduce the energy consumption of electrical loads. The aggregated electricity generations of non-intermittent and intermittent electricity generation facilities were 46,439 kWh and 3135 kWh, respectively. As shown in Fig. 14 (b), the aggregated heating energy transactions of MGs with the energy system were 537 kWh. Further, the aggregated heating energy consumptions of MGs without and with IBDRP1 were 19,353 kWh and 19,140 kWh, respectively. Thus, the IBDRP1 reduced the heating energy consumption by about 1.1%. The boilers produced heating energy without and with the IBDRP1 process by about 17,954 kWh and 17,805 kWh, respectively. Further, the absorption chillers consumed heating energy by about 10,120 kWh and 9648 kWh without and with the IBDRP1 process, respectively.

Based on Fig. 14 (c), the aggregated cooling energy transactions of MGs with the energy system was 482 kWh. Furthermore, the aggregated cooling energy consumptions of MGs without and with IBDRP1 were 12,096 kWh and 11,912 kWh, respectively. It can be concluded that the IBDRP1 reduced the cooling energy consumption by about 1.51%. The compression chillers produced 1975 kWh and 2746 kWh of cooling energy without and with the IBDRP1 process, respectively. However, the cooling energy generation of absorption chillers was reduced by about 4.67% concerning without the IBDRP1 case.

Fig. 15 (a), (b), and (c) depict the aggregated values of optimal day-ahead electrical, heating, and cooling distributed energy resources of MGs for the IBDRP2 case, respectively. As shown in Fig. 15 (a), the aggregated electricity transaction of MGs with the energy system was 1500 kWh. Thus, the IBDRP2 process increased the electricity transactions of MGs with the energy system by about 0.43% concerning the IBDRP1 electricity transactions. The aggregated electricity consumptions of MGs without and with IBDRP2 were 48,384 kWh and 48,384 kWh, respectively. The IBDRP2 process did not reduce the energy consumption of electrical loads. The aggregated electricity generations of non-intermittent and intermittent electricity generation facilities were 46,326 kWh and 3174 kWh, respectively. Thus, the IBDRP2 process reduced the energy generation of non-intermittent electricity generation facilities by about 0.24% and increased the commitment of energy storage-based intermittent electricity generation facilities by about 1.23% concerning the IBDRP1 case.

As shown in Fig. 15 (b), the aggregated heating energy transaction of MGs with the energy system was 822 kWh. Thus, the IBDRP2 process increased the heating energy transactions of MGs with the energy system by about 53.02% concerning the IBDRP1 case. Furthermore, the aggregated heating energy consumptions of MGs without and with IBDRP2 were 19,353 kWh and 19,572 kWh, respectively. Thus, the IBDRP2 increased the heating energy consumption by about 1.12%, based on the fact that the proposed demand response tariff encouraged MGs to consume more heating energy at off-peak periods. The boilers produced heating energy without and with the IBDRP2 process by about 17,954 kWh and 18,522 kWh, respectively.

Based on Fig. 15 (c) results, the aggregated cooling energy transactions of MGs with the energy system was 684 kWh. Thus, the IBDRP2 process increased the cooling energy transactions of MGs with the energy system by about 42.08% concerning the IBDRP1 case. The aggregated cooling energy consumptions of MGs without and with IBDRP2 were 12,096 kWh and 12,048 kWh, respectively. Thus, the IBDRP2 reduced the cooling energy consumption by about 0.39%. The compression chillers produced 1975 kWh and 3084 kWh of cooling energy without and with the IBDRP2 process, respectively. Thus, the cooling energy generation of compression chillers was increased by about 56.15% concerning without the IBDRP1 case.

Fig. 16 (a), (b), and (c) present the aggregated values of optimal day-ahead electrical, heating, and cooling distributed energy resources of the energy system for the IBDRP2 case, respectively. The aggregated electricity transactions of MGs with the energy system before and after the IBDRP2 process were 177 MWh and 146 MWh, respectively, as shown in Fig. 16 (a). Thus, the IBDRP2 process decreased the electricity transactions of the energy system with the wholesale electricity market by about 17.7% concerning the no-demand response case. The aggregated electricity consumptions of the energy system without and with IBDRP2 were 294 MWh and 286 MWh, respectively. The IBDRP2 process decreased the energy consumption of energy system electrical loads by about 2.75%. The aggregated electricity generations of non-intermittent electricity generation facilities were 170 MWh and 146 MWh, respectively. Thus, the IBDRP2 mechanism reduced the energy generation of non-intermittent electricity generation facilities by about 14%.

Based on Fig. 16 (b) results, the aggregated heating energy transactions of the energy system with the heating energy market before and after the IBDRP2 process were 11.28 MWh and 5.58 MWh, respectively. Thus, the IBDRP2 process decreased the heating energy transactions of the energy system with the heating energy market by about 50.53%. Further, the aggregated heating energy consumptions of the energy system without and with the IBDRP2 process were 367.77 MWh and 348.03 MWh, respectively. Thus, the IBDRP2 decreased the heating energy consumption by about 5.53%. The boilers produced heating energy without and with the IBDRP2 process by about 183.35 MWh and 169.31 MWh, respectively.

The aggregated cooling energy transactions of the energy system with the cooling energy market before and after the IBDRP2 process were 12.18 MWh and 9.33 MWh, respectively, as shown in Fig. 16 (c). It can be concluded that the IBDRP2 process decreased the cooling energy transactions of the energy system with the cooling energy market by about 23.39%. Furthermore, the aggregated cooling energy consumptions of the energy system without and with the IBDRP2 process were 146.38 MWh and 139.46 MWh, respectively. Thus, the IBDRP2 decreased the cooling energy consumption by about 4.72%.

Fig. 17 (a), (b), and (c) present the optimal day-ahead dispatch of cooling energy storage, heating energy storage, and PHEV parking lots of the energy system for the IBDRP2 case, respectively.

The maximum and minimum values of heating energy storage heating energy transactions with the energy system were 96 kWh and 32 kWh, respectively. Further, the average value of day-ahead heating energy transactions of heating energy storage facilities was 80 kWh. The maximum and minimum values of cooling energy storage cooling energy transactions with the energy system were 96 kWh and 30 kWh, respectively. Further, the average value of day-ahead cooling energy transactions of cooling energy storage facilities was 76 kWh. Finally, the maximum and minimum values of PHEV parking lots' electricity transactions with the energy system were 444 kWh and 163 kWh, respectively. Further, the average value of day-ahead electricity transactions of PHEV parking lots was 125 kWh.

Fig. 18 (a) and Fig. 18 (b) present the day-ahead and real-time cost/benefit of energy system transactions with the multicarrier energy markets for the IBDRP2 process, respectively. As shown in Fig. 18 (a), the energy system's benefits for transactions with the day-ahead electricity, heating, and cooling markets were 0.635 MMUs, −8910.1 MUs, and −18512.3 MUs, respectively. Further, as shown in Fig. 18 (b) the energy system benefits for transactions with the real-time electricity, heating, and cooling markets were 1.27 MMUs, −0.139 MMUs, and −36715.2 MUs, respectively. Thus, the aggregated benefits of the energy system in the day-ahead and real-time markets were 0.61 MMUs and 1.10 MMUs, respectively; meanwhile, the energy system operational costs were about 0.49 MMUs and 0.63 MMUs in the day-ahead and real-time markets, respectively concerning no energy transactions with energy markets. Hence, the proposed method increased the benefits of the

energy system using energy transactions with the day-ahead and real-time markets.

Fig. 19 depicts the resiliency index of the energy system for the worst-case shock conditions considering different demand response programs and without the proposed method. As shown in Fig. 19, the IBDRP2 process provided a higher resiliency index. The resiliency index of the energy system tends to infinity using the proposed method for the worst-case shock scenario.

Fig. 20 shows the optimal topology number of the energy system for the real-time optimization process for different demand response alternatives and the corresponding worst-case shock.

Fig. 21 (a), (b), and (c) present the optimal real-time dispatch of electrical, heating, and cooling distributed energy systems of the energy system for IBDRP2, respectively considering the worst-case shock impact on the system. As mentioned earlier, the worst-case scenario occurred in energy corridor 160 at 15:00 and the second shock happened in energy corridor 135 at 19:00.

The CHPs of the energy system continuously produced electricity by about 7.214 MW before and after external shocks, as shown in Fig. 21 (a). However, the electricity generation of DGs reduced from 9.17 MW to 7.47 MW for the first shock. Further, when the second shock occurred, the electricity generation of DGs increased from 4.98 MW to 5.51 MW for the second shock. The aggregated and average electricity consumptions of the system were 970.86 MWh and 10.12 MW, respectively for normal conditions. However, the aggregated and average electricity consumptions of the system were 928.30 MWh and 9.57 MW, respectively. Thus, the IBDRP2 decreased the aggregated and average electricity consumption of the system by about 4.38% and 5.24%, respectively. Further, the aggregated and average electricity transactions of the energy system with the wholesale electricity market were 724.65 MWh and 7.47 MW, respectively for normal conditions. Finally, the aggregated and average electricity transactions of the energy system with the wholesale electricity market were 758.72 MWh and 7.82 MW, respectively for shock conditions. Thus, the shock conditions increased the electricity transactions of the energy system with the wholesale electricity market by about 4.7%.

Based on Fig. 21 (b) results, the aggregated and average heating energy consumptions of the system were 1243.73 MWh and 12.82 MW, respectively for normal conditions. However, the aggregated and average heating energy consumptions of the energy system were 1163.30 MWh and 11.99 MW, respectively. Thus, the proposed process decreased the aggregated and average heating energy consumption of the system by about 6.47% and 6.42%, respectively. Further, the aggregated and average heating energy transactions of the energy system with the heating energy market were 31.67 MWh and 0.33 MW, respectively for normal conditions. Finally, the aggregated and average heating energy transactions of the energy system with the heating energy market were 66.71 MWh and 0.69 MW, respectively for shock conditions. Thus, the shock conditions increased the heating energy transactions of the energy system with the heating energy market by about 52.53%.

The aggregated and average cooling energy consumptions of the system were 491.32 MWh and 5.06 MW, respectively for normal conditions, based on Fig. 21 (c) results. The aggregated and average cooling energy consumptions of the system were 461.61 MWh and 4.75 MW, respectively. Thus, the proposed model decreased the aggregated and average cooling energy consumption of the system by about 6.04% and 6.12%, respectively. Further, the aggregated and average cooling energy transactions of the energy system with the cooling energy market were 344.64 MWh and 3.55 MW, respectively for normal conditions. Finally, the aggregated and average cooling energy transactions of the energy system with the cooling energy market were 287.49 MWh and 2.96 MW, respectively for shock conditions. Thus, the shock conditions decreased the cooling energy transactions of the energy system with the cooling energy market by about 16.58%.

In conclusion, the proposed model successfully determines the optimum commitment of multi-carrier MGs, energy system DERs scheduling, and the topology of the system for normal and external shock conditions.

5. Conclusion

This paper proposed a framework for day-ahead and real-time scheduling of microgrids and the energy distribution system that transacted multi-carrier energy with each other in normal and shock conditions. The energy system also transacted electrical, heating, and cooling energy carriers with wholesale electricity market, heating energy market, and cooling markets, respectively.

The proposed method calculated the resiliency index of the energy system and determined the optimal status of electrical switches, heating, and cooling control valves to enhance the resiliency of the system. The two-stage two-level optimization model determines the scheduling of the energy system and microgrids considering the incentive-based and price-based demand response procedures. The proposed method was simulated for the 123-bus test system. The proposed incentive-based demand response process successfully reduced the aggregated and average electricity consumption of the system by about 4.38% and 5.24%, respectively. Further, the proposed process decreased the aggregated heating and cooling energy consumption of the system by about 6.47% and 6.04%, respectively. The authors are working on the modeling of a hydrogen energy carrier system to integrate with the proposed model.

References

[1] Jiang Tao, Dong Xinru, Zhang Rufeng, Li Xue. Strategic active and reactive power scheduling of integrated community energy systems in day-ahead distribution electricity market. Appl Energy 2023;336:120558.

[2] Xiao Min, Smaisim Ghassan Fadhil. Joint chance-constrained multi-objective optimal function of multi-energy microgrid containing energy storages and carbon recycling system. J Energy Stor 2022;55:105842.

[3] Pang Kang Ying, Liew Peng Yen, Woon Kok Sin, Ho Wai Shin, Alwi Sharifah Rafidah Wan, Klemes Jirí Jaromír. Multi-period multi-objective optimisation model for multi-energy urban-industrial symbiosis with heat, cooling, power and hydrogen demands. Energy 2023;262:125201.

[4] Li Yaowang, Yao Fuxing, Zhang Shixu, Liu Yuliang, Miao Shihong. An optimal dispatch model of adiabatic compressed air energy storage system considering its temperature dynamic behavior for combined cooling, heating and power microgrid dispatch. J Energy Stor 2022;51:104366.

[5] Zhang Zhiyang, Altalbawy Farag MA, Al-Bahrani Mohammed, Riadi Yassine. Regret-based multi-objective optimization of carbon capture facility in CHP-based microgrid with carbon dioxide cycling. J Clean Prod 2023;384:135632.

[6] Mianaei Peyman Khorshidian, Aliahmadi Mohammad, Faghri Safura, Ensaf Mohammad, Ghasemi Amir, Abdoos Ali Akbar. Chance-constrained

programming for optimal scheduling of combined cooling, heating, and power-based microgrid coupled with flexible technologies. Sustain Cities Soc 2022;77:103502.

[7] Vahedipour-Dahraie Mostafa, Rashidizadeh-Kermani Homa, Anvari-Moghaddam Amjad, Siano Pierluigi, Catalao Joao PS. Short-term reliability and economic evaluation of resilient microgrids under incentive-based demand response programs. Electr Power Energy Syst 2022;138:107918.

[8] Guo Jiqun, Tan Jinjing, Li Yang, Haifei Gu, Liu Xin, Cao Yang, et al. Decentralized incentive-based multi-energy trading mechanism for CCHP-based MG cluster. Electr Power Energy Syst 2021;133:107138.

[9] Guo Qun, Nojavan Sayyad, Lei Shi, Liang Xiaodan. Economic-environmental evaluation of industrial energy parks integrated with CCHP units under a hybrid IGDT-stochastic optimization approach. J Clean Prod 2021;317:128364.

[10] Lekvan Amir Aris, Habibifar Reza, Moradi Mehran, Khoshjahan Mohammad, Nojavan Sayyad, Jermsittiparsert Kittisak. Robust optimization of renewable-based multi-energy micro-grid integrated with flexible energy conversion and storage devices. Sustain Cities Soc 2021;64:102532.

[11] Li Ke, Wei Xingguo, Yan Yi, Zhang Chenghui. Bi-level optimization design strategy for compressed air energy storage of a combined cooling, heating, and power system. J Energy Stor 2020;31:101642.

[12] Saberi Kasra, Pashaei-Didani Hamed, Nourollahi Ramin, Zare Kazem. Optimal performance of CCHP based microgrid considering environmental issue in the presence of real time demand response. Sustain Cities Soc 2019;45:596–606.

[13] Zhou Xiaoqian, Ai Qian. Distributed economic and environmental dispatch in two kinds of CCHP microgrid clusters. Electr Power Energy Syst 2019;112:109–26.

[14] Tooryan Fatemeh, HassanzadehFard Hamid, Dargahi Vahid, Jin Shuangshuang. A cost-effective approach for optimal energy management of a hybrid CCHP microgrid with different hydrogen production considering load growth analysis. Int J Hydrogen Energy 2022;47:6569–85.

[15] Luo Zhao, Zhi Wu, Li Zhenyuan, Cai HongYi, Li BaoJu, Gu Wei. A two-stage optimization and control for CCHP microgrid energy management. Appl Therm Eng 2017;125:513–22.

[16] Fazlhashemi Seyed Saeed, Sedighizadeh Mostafa, Khodayar Mohammad E. Day-ahead energy management and feeder reconfiguration for microgrids with CCHP and energy storage systems. J Energy Stor 2020;29:101301.

[17] Cheng Zhiping, Jia Dongqiang, Li Zhongwen, Si Jikai, Xu Shuai. Multi-time scale dynamic robust optimal scheduling of CCHP microgrid based on rolling optimization. Electr Power Energy Syst 2022;139:107957.

[18] Chen Lingmin Wu, Jiekang Tang Huiling, Feng Jin, Yanan Wang. A Q-learning based optimization method of energy management for peak load control of residential areas with CCHP systems. Electr Pow Syst Res 2023;214:108895.

[19] Chen Lingmin, Tang Huiling, Jiekang Wu, Li Changjie, Wang Yanan. A robust optimization framework for energy management of CCHP users with integrated demand response in electricity market. Electr Power Energy Syst 2022;141:108181.

[20] Zhai Junyi, Wang Sheng, Guo Lei, Jiang Yuning, Kang Zhongjian, Jones Colin N. Data-driven distributionally robust joint chance-constrained energy management for multi-energy microgrid. Appl Energy 2022;326:119939.

[21] Yang Xiaohui, Leng Zhengyang, Shaoping Xu, Yang Chunsheng, Yang Li, Liu Kang, et al. Multi-objective optimal scheduling for CCHP microgrids considering peak-load reduction by augmented ε-constraint method. Renew Energy 2021;172:408–23.

[22] Zheng Nan, Zhang Hanfei, Duan Liqiang, Wang Xiaomeng, Wang Qiushi, Liu Luyao. Multi-criteria performance analysis and optimization of a solar-driven CCHP system based on PEMWE, SOFC, TES, and novel PVT for hotel and office buildings. Renew Energy 2023;206:1249–64.

[23] Varasteh Farid, Nazar Mehrdad Setayesh, Heidari Alireza, Shafie-khah Miadreza, Catalão Joao PS. Distributed energy resource and network expansion planning of a CCHP based active microgrid considering demand response programs. Energy 2019;172:79–105.

[24] Zakernezhad H, Setayesh Nazar M, Shafie-khah MR, Catalão JPS. Optimal resilient operation of multi-carrier energy systems in electricity markets considering distributed energy resource aggregators. Appl Energy 2021;299:117271.

[25] Aghajani R, Shayanfar HA, Shayeghi H. Demand side management in a smart micro-grid in the presence of renewable generation and demand response. Energy 2017;126:622–37.

[26] Box GEP, Jenkins GM, Reinsel GC. Time series analysis. John Wiley & Sons; 2013.

[27] Heitsch H, Romisch W. Scenario reduction algorithms in stochastic programming. Comput Optim Appl 2003;24(2):187–206.

[28] Jiang Qiangqiang, Cai Baoping, Zhang Yanping, Xie Min, Liu Cuiwei. Resilience assessment methodology of natural gas network system under random leakage. Reliab Eng Syst Safety 2023;234:109134.

[29] Thomopoulos Nick T. Essentials of Monte Carlo simulation statistical methods for building simulation models. New York: Springer-Verlag; 2013.